

Technical Design Report for
the MiniBooNE Neutrino Beam

May 13, 2001

I. Stancu

University of Alabama, Tuscaloosa, AL 35487

S. Koutsoliotas

Bucknell University, Lewisburg, PA 17837

E. Church, G. J. VanDalen

University of California, Riverside, CA 92521

R. A. Johnson, J. L. Raaf, N. Suwonjandee

University of Cincinnati, Cincinnati, OH 45221

L. Bugel, J. M. Conrad, B. T. Fleming, J. Formaggio,

M. H. Shaevitz, M. Sorel, E. D. Zimmerman

Columbia University, Nevis Labs, Irvington, NY 10533

D. Smith

Embry Riddle Aeronautical University, Prescott, AZ 86301

C. Bhat, S. Brice, B. C. Brown, R. Ford, F. G. Garcia, P. Kasper,
T. Kobilarcik, I. Kourbanis, A. Malensek, W. Marsh, P. Martin, F. Mills,
C. Moore, P. Nienaber, A. Russell, P. Spentzouris, R. Stefanski, T. Williams

Fermi National Accelerator Laboratory, Batavia, IL 60510

R. Tayloe

Indiana University, Bloomington, IN 47405

G. T. Garvey, E. Hawker, W. C. Louis, G. B. Mills, V. Sandberg,

B. Sapp, R. Schirato, R. Van de Water, D. H. White

Los Alamos National Laboratory, Los Alamos, NM 87545

R. Imlay, W. Metcalf, M. Sung, M. Wascko

Louisiana State University, Baton Rouge, LA 70803

B. P. Roe

University of Michigan, Ann Arbor, MI 48109

A. O. Bazarko, P. D. Meyers, F. C. Shoemaker

Princeton University, Princeton, NJ 08544

Contents

1	Overview	7
1.1	Purpose	7
1.2	Other Supporting Materials	7
1.3	Physics-driven Requirements	11
2	Interface to the 8 GeV Primary Beam	13
2.1	Water Systems (WBS 1.1.8)	13
2.2	Primary Beam Monitoring (WBS 1.1.9)	13
2.2.1	Protection of Horn from Mistuned Beam	13
2.3	Controls (WBS 1.1.10)	15
2.4	Safety Interlocks (WBS 1.1.11)	15
3	The MiniBooNE Neutrino Beam (WBS 2)	17
3.1	Target Hall (WBS 2.3.1)	17
3.2	Shielding, Decay Pipe, and Absorbers (WBS 2.1.9)	17
3.2.1	Beam Absorber Design (WBS 2.1.7, 2.1.9)	17
3.2.2	Little Muon Counters	21
3.2.3	Target Pile (WBS 2.1.8)	21
3.3	Horn and Target (WBS 2.1)	28
3.3.1	Horn specifics	29
3.3.2	The Finite Element Analyses of the Horn (WBS 2.1.4)	32
3.3.3	Cooling of the Horn (WBS 2.1.3, 2.1.10)	32
3.3.4	The Modal Finite Element Analyses of the Horn and Fourier Analysis of the Vibration Power Spectrum (WBS 2.1.3)	38
3.3.5	The Beryllium Target Assembly (WBS 2.1.5)	40
3.3.6	The Target Support Interface (WBS 2.1.6)	42
3.3.7	Horn Power Supply (WBS 2.1.11)	44
4	The Neutrino Flux	49
4.1	The ν_μ Flux	49
4.2	The ν_e Background	49
4.3	Comparison to the Design Goal	53
5	Radiation Safety and Hazard Analysis	55
5.1	Prompt Radiation	55
5.1.1	The 8 GeV Beamline	57
5.1.2	The MiniBooNE Neutrino Beam	57
5.2	Residual Radioactivity	58
5.2.1	Evaluation of Residual Activity	58
5.2.2	Safe Handling of Irradiated Horns	58

5.3	Air Activation	62
5.3.1	Summary of Regulatory Requirements	63
5.4	Ground Water Contamination	64
5.5	Surface Water Contamination	68

DRAFT

List of Tables

1.1	The highest level Work Breakdown Structure for the projects associated with MiniBooNE. . .	8
1.2	This table assumes that a 600 event excess is observed in the first half of the MiniBooNE run, with a 50 m decay length (line 1). Then for the second half run, with absorber at the 25 m position, the predicted event rate for oscillations is compared to ν_e beam background (line 2).	12
3.1	Properties of Aluminum Alloy 6061-T6.	29
3.2	Properties of beryllium	40
3.3	A breakdown of energy deposition sources in the beryllium target	42
3.4	Horn circuit characteristics	46
5.1	Maximum residual activity of various locations in the MiniBooNE target region, decay region, and beamline elements at contact. Ten years' irradiation and one day cooldown have been assumed. The statistical errors in these predicted dose rates are of the order of 15%.	61

List of Figures

1.1	A schematic view of the 8 GeV Fixed Target Facility, the neutrino beam, and the MiniBooNE detector.	9
1.2	The Target Hall, and the Decay Pipe.	10
2.1	Schematic overview of location of instrumentation in the primary proton beamline. Key LM: – loss monitor, VT – vertical trim, HT – horizontal trim, MW – multiwire, Tor – toroid, bpm – beam position monitor.	14
3.1	An overview of the MiniBooNE Projects showing the portion described in Chapter 3 by the shaded area.	18
3.2	Below-grade plan view of the 8 GeV beam tunnel. Enlarged versions available in reference [5].	18
3.3	Beam profiles showing the growth in size as the 8 GeV proton beam drifts through the Decay Pipe for a 20π beam.	19
3.4	Beam profiles showing the growth in size as the 8 GeV proton beam drifts through the Decay Pipe for a 40π beam.	20
3.5	A schematic diagram of the Lab E steel plates that will be used for the 25 m beam absorber. Protrusions will be removed.	22
3.6	Above-grade plan view of the Target Hall, decay pipe and absorbers. Enlarged versions available in reference [5].	23
3.7	Below-grade plan view of the Target Hall, decay pipe and absorbers. Enlarged versions available in reference [5].	23
3.8	Sections showing the 25m absorber silo and the installation process.	24
3.9	An elevation view of the target pile, including the horn, adjuster module, shielding steel. The stripline extends upward at the left.	25
3.10	View showing the stripline coming down from the power supply in the surface building (building not shown), through vertical penetrations, and down to the horn in the shielding vault below ground. The concrete and steel shielding around the horn is not shown for clarity. . . .	26
3.11	Horn in box with air-tightening cover suspended above. The thin Al downstream window is not shown so that the horn can be seen through the aperture.	27
3.12	Side view of the horn, stripline and target with the horn box rendered transparent.	30
3.13	Stripline connection to the upstream end of the horn.	30
3.14	Exploded view of the upstream connection between the outer conductor, ceramic ring, and inner conductor.	31
3.15	Outer view of the assembled horn and water truss.	31
3.16	Graph of the number of cycles to failure for Al 6061-T6 vs equivalent stress in ksi. Different curves represent different confidence levels.	33
3.17	Graph of ratio of calculated stress to allowable stress vs element number.	34
3.18	Graph of average heat transfer coefficient vs water pressure and number of spray nozzles in operation azimuthally.	36

3.19	A view of a single spray nozzle with its vibration isolation bellows. The bellows and OC are transparent to see the nozzle tube.	37
3.20	Side view of horn with the water system support truss. The outer conductor is rendered transparent here to see the spacing the of the cooling nozzles along the inner conductor. . . .	37
3.21	The Fourier spectrum of the MiniBooNE current pulse (ignoring the fine structure caused by the Booster cycle).	38
3.22	The first four modes and natural frequencies of the horn with no spiders. The amplitude is greatly exaggerated for illustration.	39
3.23	A drawing of the beryllium target assembly.	41
3.24	Stripline and beam pipe upstream of horn. The OC, IC and portions of the hornbox are rendered transparent to see the target insertion inside the horn.	43
3.25	Close-up of the ceramic tubes and breaks that support the target and electrically isolate it from the support structure and incoming air cooling tubes.	44
3.26	Overall view of the target module with man for scale. The right C-channel is rendered transparent to see the air tube routing inside the module.	45
3.27	A LC discharge circuit that will achieve the peak current when the LCR switch releases stored energy from the capacitor bank into the horns via the stripline	46
3.28	Current and voltage waveforms of a typical cycle of power supply operation	47
4.1	The ν_μ flux (solid) at the MiniBooNE detector compared to the ν_e background (dashed). . .	50
4.2	The ν_μ flux for the MiniBooNE horn system (dashed) compared to perfect focusing (solid). .	51
4.3	The energy dependence of the ν_e beam background compared to a hypothetical oscillation signal. The parameters for the signal are $\Delta m^2=0.4$ eV ² and $\sin^2 2\theta = 0.04$. The statistical fluctuations in the background histograms reflect limited Monte Carlo statistics; the error bars on the signal points indicate the size of the expected statistical error with 10^{21} protons on target.	52
4.4	The sensitivity of the MiniBooNE designed beam compared to the final results from LSND. The solid curve represents the expected 90% confidence level limit from E898 if there is no signal. The analysis removes events with an equivalent electron energy greater than 1 GeV. The sensitivity from the original E898 proposal is shown as the dashed curve.	54
5.1	Top: Nuclear star density as a function of distance from wall of Decay Pipe as calculated by GEANT. Bottom: Position where propagated neutrons stop.	56
5.2	Energy distribution of stars as calculated by GEANT.	57
5.3	Nuclear star density as a function of radius r in the steel of the Target Pile, as calculated by CASIM, providing confirmation of the MARS results.	59
5.4	Predicted radiation dose in the surface layers of the Target Pile steel and decay region. . . .	60
5.5	MARS calculated star densities in the decay volume.	65
5.6	CASIM calculation of star density as a function of radius (azimuthally integrated) throughout the target and decay region. The absorber is at $Z=5000$ cm.	66
5.7	Equilibrium concentrations of tritium as a function of radius in the decay volume.	66
5.8	Equilibrium concentrations of ²² Na as a function of radius in the decay volume.	67

Chapter 1

Overview

This Technical Design Report (TDR) describes the components associated with the neutrino beam for BooNE, the Booster Neutrino Experiment[1]. The first phase of BooNE, called “MiniBooNE” or E898, was given Stage I approval by the Director of Fermilab on May 15, 1998. MiniBooNE is searching for $\nu_\mu \rightarrow \nu_e$ oscillations, identified through $\nu_e C \rightarrow e^- N$ quasi-elastic scattering in the detector. Created with the express purpose of investigating the LSND effect [2] discovered at LANL, the experiment will have exceptional sensitivity in the LSND region of parameter space and will be capable of carrying out a definitive measurement of the LSND effect.

1.1 Purpose

There are two geographically separate parts of the MiniBooNE project, as shown in Figure 1.1.

1. The Neutrino Beam devices are enclosed in the Target Hall, the Target Service Building, and the Decay Region, and consist of all of the technical elements required to form a neutrino beam. This includes the horn (focusing system) and power supply, the target and target shielding, and the beam absorbers.
2. The detector is a 40' diameter, mineral oil Čerenkov detector buried so that its top is at grade level. This detector uses 1500 phototubes to detect charged particles created in neutrino interactions.

The purpose of this document is to describe the technical design of components in the neutrino beam. The Detector is described in a separate TDR [3]. Section 1.2 lists other documents supporting this project. Figure 1.2 gives a more detailed view of the 8 GeV Beam enclosures and the MiniBooNE Target Hall.

This report follows the Work Breakdown Structure (WBS), with a reference at the head of each chapter and each relevant section. To build these Facilities, Fermilab will engage in a MiniBooNE AIP. Construction of the horn and radiation shields are done as Equipment or Operating projects. Within the WBS structure, the MiniBooNE Projects are WBS 2. Table 1.1 gives the highest level WBS for MiniBooNE.

1.2 Other Supporting Materials

This document focuses entirely on neutrino beam elements and enclosures. Other supporting materials for the BooNE Experiment and the 8 GeV Fixed Target Facility are:

- *The MiniBooNE Proposal* [1] which was approved in May, 1998. The physics of MiniBooNE is reviewed. The salient issues of flux and background are described in detail. The design of the experiment (both beam and detector) remains unchanged at the gross level. However, details of design are superseded by the Technical Design Reports.

Table 1.1: The highest level Work Breakdown Structure for the projects associated with MiniBooNE.

WBS #	Title
2.	MiniBooNE
2.1	MiniBooNE Equipment (EQ)
2.1.1	Horn Assembly Tooling
2.1.2	Prototype Horn Beamline Box
2.1.3	Pre-Prototype Horn Project
2.1.4	Prototype Horn Short Stripline
2.1.5	Target Development and Fabrication
2.1.6	Target/BPM Support-Alignment System
2.1.7	Muon Monitor Modules
2.1.8	Target Pile
2.1.9	25 Meter Absorber
2.1.10	MiniBooNE Water Systems
2.1.11	Horn Power Supply
2.1.12	Horn Adjustor Module
2.1.13	HH & Target Containment Vessels an Support Structures
2.1.14	Stripline System
2.1.15	Prototype Horn
2.1.16	Production Horn
2.2	The MiniBooNE Detector
2.3	Civil Construction
2.3.1	Target Hall & Decay Pipe
2.3.2	Detector Enclosure

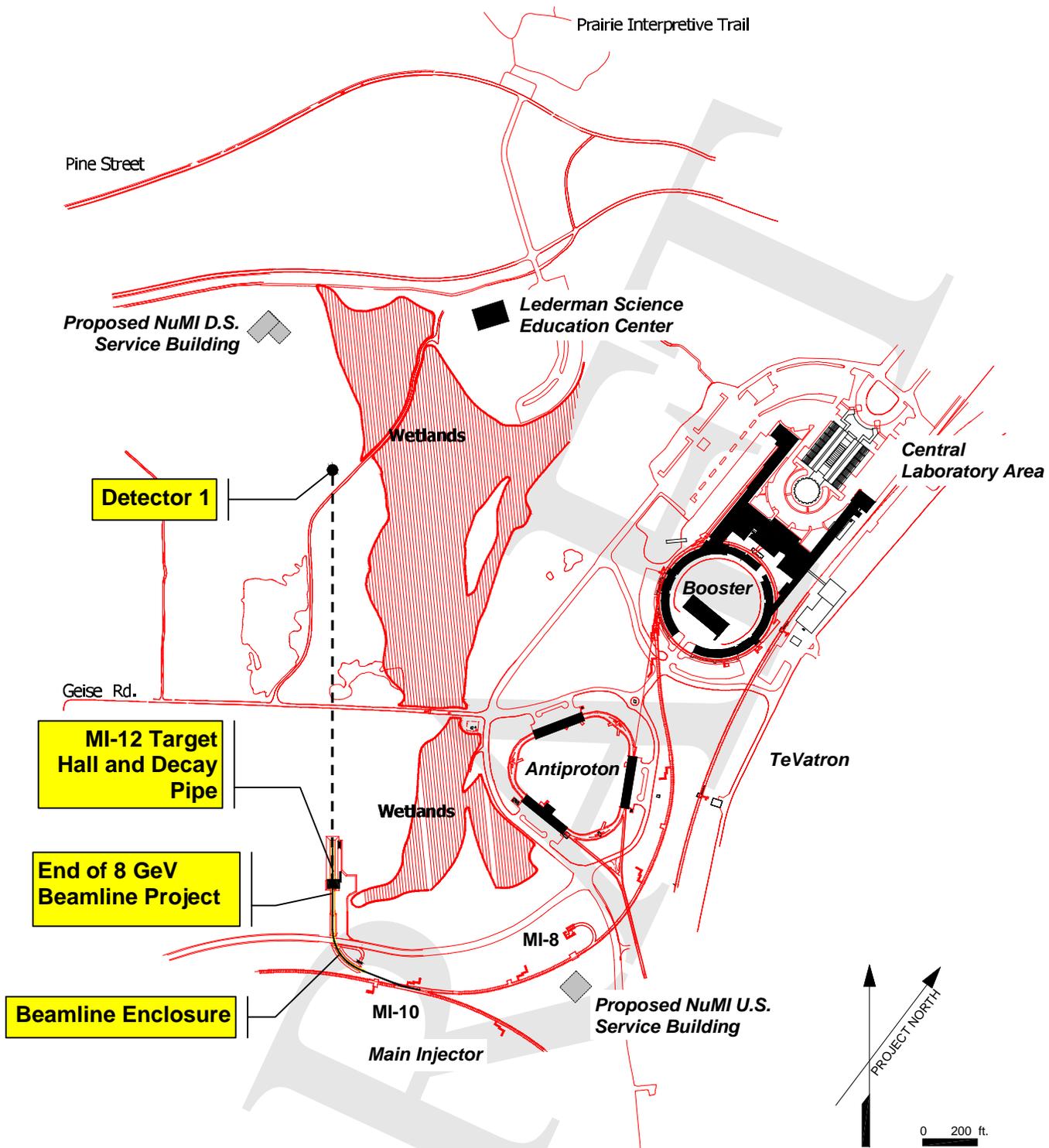


Figure 1.1: A schematic view of the 8 GeV Fixed Target Facility, the neutrino beam, and the MiniBooNE detector.

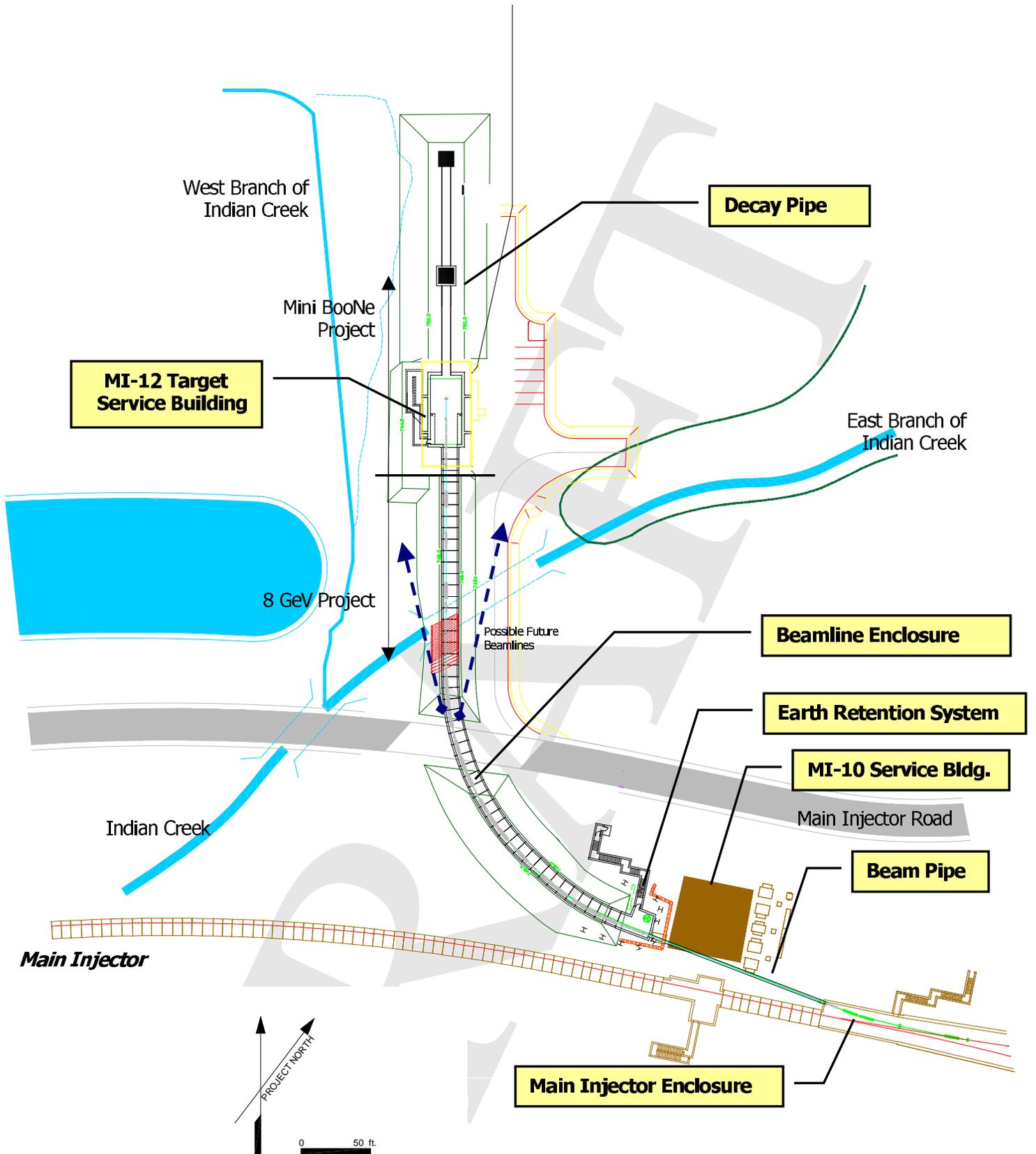


Figure 1.2: Target Hall, Target Service Building and Decay Pipe.

- *The Environmental Assessment (EA)* [4] which describes the environmental impact of the MiniBooNE running. In this document, project areas 1 and 2 (the 8 GeV Beam and the BooNE Neutrino Beam) are considered together, under the title, “The 8 GeV Fixed Target Facility,” because of their geographic proximity and inter-related environmental issues.
- *The Conceptual Design Reports (CDR)* [5] which describe the construction of the Target Hall, and detector enclosure for BooNE.
- *The MiniBooNE Detector TDR* [3] which describes the technical components of the detector.
- *The 8 GeV Beam TDR* [3] which describes the technical components of the 8 GeV Beamline.
- *A Memorandum of Understanding (MOU)* [6] which describes the organization and set of responsibilities for building the detector.
- *The Preliminary Safety Assessment Document (PSAD)* [7] which contains hazard analyses for the MiniBooNE Facilities.
- *The Project Management Plan (PMP)* [8] which describes the organization and responsibilities for the construction, including technical beam elements.
- *The MiniBooNE Cost Books* [9] which contain cost and schedule information. Costbook 1 covers all but WBS 2.2 (detector internals). Costbook 2 covers the detector.

1.3 Physics-driven Requirements

The physics-driven design requirements are: a low energy ν_μ beam of high intensity with low ν_e contamination and well understood spectrum. For detailed explanations of the design issues discussed in the section, see the MiniBooNE proposal [1].

The probability for oscillations is given by:

$$P = \sin^2 2\theta \sin^2(1.27\Delta m^2 L/E), \quad (1.1)$$

where θ and Δm^2 (in eV^2) are the fundamental parameters to be measured and L and E are the distance from the neutrino source to the detector and the energy of the neutrino, respectively. The ratio L/E (in units of m/MeV or km/GeV) regulates the experimental sensitivity to Δm^2 . The LSND oscillation allowed region corresponds to L/E near 1 km/GeV ; for the LSND decay-at-rest analysis, $E \sim 20$ to 60 MeV and $L = 30 \text{ m}$.

MiniBooNE was designed with L and E values which are over an order of magnitude larger than LSND, while maintaining $L/E \sim 1 \text{ km/GeV}$, in order to change substantially the production systematics while maintaining sensitivity. Given that the L and E values should be approximately $\times 10$ larger than the LSND design, FNAL offers an optimal site. The Booster protons can be used to produce a neutrino beam of low energies, with a high flux between 0.3 and 1 GeV . The corresponding L value of $\sim 500 \text{ m}$ easily fits on the FNAL site. The site was chosen to allow a second detector to be placed anywhere from 250 m to 2 km if a signal is observed, permitting precise measurements of the oscillation parameters.

LSND has observed an excess of 39.5 ± 8.8 events (*preliminary, 1993-1998*)[11]. The MiniBooNE goal is to obtain over an order of magnitude higher statistics. This will assure that the signal is decisive. Therefore, high intensity is a crucial design goal. The high intensity will drive shielding and absorber design. Intensity issues fall into two categories related to the active devices: Booster delivery of protons on target and meson focusing.

The Booster is a high-intensity proton source. MiniBooNE requires protons from the Booster at a rate of 5 Hz with 5×10^{12} protons per pulse at 8 GeV for 4×10^7 seconds of Booster running (1.33 calendar years or 10^{21} protons on target). As described in Ref. [12], these goals are relatively conservative and should

Decay Pipe Length (m)	ν_μ events	If excess is $\nu_\mu \rightarrow \nu_e$ oscillation	If excess is due to ν_e bkgnd
50 (initial 1/2 run)	700,000	600 ± 50	600 ± 50
25 (final 1/2 run)	390,000	334 ± 35	174 ± 32

Table 1.2: This table assumes that a 600 event excess is observed in the first half of the MiniBooNE run, with a 50 m decay length (line 1). Then for the second half run, with absorber at the 25 m position, the predicted event rate for oscillations is compared to ν_e beam background (line 2).

be achievable. The initial run will begin in late 2001 and end before the start of the NuMI run, currently scheduled to begin in November, 2002.

In designing the decay region, the physics issues are: a) maximize the ν_μ flux below 1 GeV, b) minimize the ν_e flux, and c) understand well the systematics of the ν_e flux. Maintaining a high flux places design constraints on the primary beam at the target of < 1 mm position stability, < 4.6 mrad angular stability and < 5 mm 1/2 spot size (95% contained), as described in the primary beam Technical Design Report. The experiment uses a meson focusing system which optimizes the flux of neutrinos incident on the detector. This horn system differs from previous neutrino horn systems because it is designed for energies below 1 GeV and operates at a cycle rate up to 7.5 Hz. The flux from the neutrino horn is discussed in Section 3.3. The ν_e flux contributions from μ decay and K decay are roughly equal. Lengthening the decay pipe produces a higher ν_μ flux, but also a higher background. Studies have shown that satisfactory lengths are in the range 25 to 50m [1]. The decay pipe will be filled with air and capped at each end. Maintaining a vacuum in the pipe would result in only a 3.5% increase in flux, which was deemed too small to justify the cost and maintenance issues involved in a vacuum system.

Each source of neutrino production in MiniBooNE has a different dependence on the length of the decay pipe. First, consider the ν_e backgrounds. For ν_e 's from muons, the decay pipe length, $L = 50$ m, is much smaller than the muon decay length, $\lambda_\mu \approx 7100$ m, given the muon energies. The muon decay probability is then $\frac{(L-x)}{\lambda_\mu}$, where x is the point where the pion decays. Integrating over x from 0 to L and weighting by the pion decay probability, $\frac{e^{-\frac{x}{\lambda_\pi}}}{\lambda_\pi}$, yields a ν_e background rate that is proportional to $L^2/\lambda_\mu\lambda_\pi$.

Second, consider the oscillation signal. The $\pi_{\mu 2}$ source of detected ν_μ events and, therefore, the oscillation signal would be proportional to L since $\lambda_\pi > L$.

Finally, consider the smaller K_{e3}^+ and K_{e3}^L sources of ν_e background. Because of the short lifetime of the K^+ and the fact that K_L are unfocused, these backgrounds occur mainly from upstream decays and have weaker dependence on L than the signal.

From this, one can see that a variation of the decay pipe length can demonstrate that an observed oscillation signal is not from a mis-estimate of a single ν_e background component. Therefore, MiniBooNE has included provision for 25m and 50m absorbers in the decay region. If an oscillation signal is observed after running with $L = 50$ m, we will change to a 25m position. A true oscillation signal should be reduced by a factor of 1.8 as opposed to a factor of 3.4 for a false signal associated with the muon decay background. An example scenario is shown in Table 1.2.

Chapter 2

Interface to the 8 GeV Primary Beam

2.1 Water Systems (WBS 1.1.8)

The cooling water for the magnets and power supplies will be provided by the Main Injector LCW system. The MI water system was designed to handle the heat load associated with a 1-second slow spill from the Main Injector, with a safety factor of approximately 20%. The “available” flow at MI-10 is estimated at 317 GPM [13]. The near term plans for the MI facility anticipate fast spill for NUMI, which requires only 45% of the power for slow spill, and under these conditions the safety factor is much larger.

The power consumption in the MiniBooNE beamline is dominated by the 6-3-120 dipoles, which account for approximately 200 kW. About 150 GPM of LCW is required for a 10° F temperature gradient. Other magnets that require LCW flow totalling approximately 50 GPM are the 3Q60, MQ, and MQA quadrupoles, and 4-4-30 trim dipoles. The power supplies, the horn RAW system, and cooling for the beam absorbers will require an additional 50 GPM. The total heat load imposed by the 8 GeV Beamline and the MiniBooNE experiment is estimated to be less than 300 GPM representing about a 10% increment to the slow-spill cycle cooling requirements at the MI-10 service building, and less than 2% of the total heat input to the cooling ponds from the ring. Neither of these increments should present a concern.

2.2 Primary Beam Monitoring (WBS 1.1.9)

The primary beam position, profile, and intensity will be monitored to maintain the highest possible flux, to constrain beam simulations, and to prevent losses. Multiwires will be used to measure beam profiles. BPMs will be used to measure beam position, and a beam current toroid will measure beam intensity. (BPMs also measure intensity, but the toroid is necessary for absolute calibration.) Since all the devices used in MiniBooNE are also used in other beamlines, spare components will be maintained by the appropriate Beams Division departments as part of the general inventory. A schematic overview of the location of beamline instrumentation is given in Figure 2.1.

2.2.1 Protection of Horn from Mistuned Beam

A “donut collimator” near the upstream end of the Target Pile, together with a loss monitor mounted on the front face of the Pile will be used to trip off the beam when it moves away from center. The purpose of these devices is to prevent mistuned beam from depositing large amounts of energy in the horn. Given the specified maximum spot size at the target, an 8 GeV beam has a maximum energy deposition in aluminum of 0.03 GeV/cm³. One pulse at 5×10^{12} would give a temperature rise of 10°C. Consider the case where the beam is mistuned in such a way that it completely misses the target. At the narrow neck of the Horn, where the beam size is roughly doubled because the beam is diverging, this implies a temperature rise on the

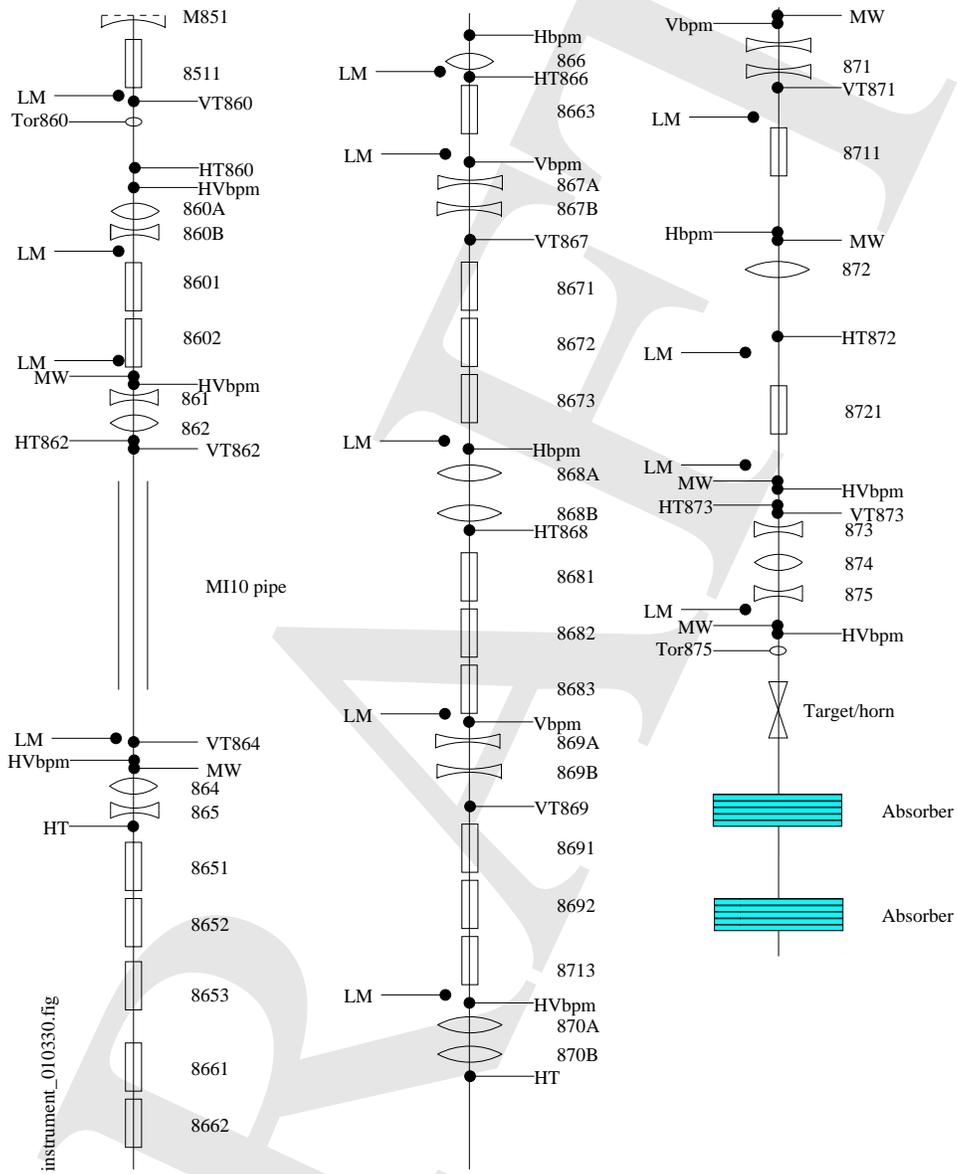


Figure 2.1: Schematic overview of location of instrumentation in the primary proton beamline. Key LM: – loss monitor, VT – vertical trim, HT – horizontal trim, MW – multiwire, Tor – toroid, bpm – beam position monitor.

conductor of 2.5 °C per pulse. Limiting the number of mistuned pulses to four, using the loss monitor, would keep the maximum temperature on the aluminum at a manageable level. The donut collimator will consist of a 5 cm long piece of copper. The outer geometry will be square, with 10 cm sides. A 3 cm diameter hole, which shadows the target, allows beam to pass through the collimator.

2.3 Controls (WBS 1.1.10)

The beam line magnets will be controlled through CAMAC modules (mostly CAMAC 453 ramp modules) and read out via CAMAC MADC's. Both of these will be connected to the Main Injector CAMAC link. The horn will be controlled and read out through an Internet Rack Monitor (IRM). BPM's and loss monitors will also be read out through IRM's. A "local application" running on an IRM will collect the BPM measurements and other time critical data (e.g. horn data) on a pulse-by-pulse (15 Hz) basis, time stamp each pulse with a GPS derived time so that the data can later be correlated with MiniBooNE detector data, and buffer this data for later access through the control system.

Multiwires and the Muon Monitor will be read out via Switchyard style SWIC scanners. These will connect like the Switchyard system to VME front end computer systems via ACNET. The VME systems will buffer the data on a pulse by pulse basis for later access through the control system. Each pulse will be time stamped with a GPS derived time stamp.

The beam line vacuum system will be controlled and monitored through the standard vacuum CIA crate. There will be one CIA crate in MI-10 which will service the entire beam line. The CIA crate will be connected to the MI vacuum front end.

Operator monitor and tuning facilities that will be needed include a BPM position display, a BPM intensity display, a loss monitor display, a multiwire display, and a ramp card setup and modification program. Many of these will be straight forward extensions to already existing code. In addition, an autotune program will be needed to keep the beam line tuned with minimal operator intervention. This program is being developed as a general facility for fixed target experiments (MiniBooNE, NUMI, 120 GeV MI fixed target). For MiniBooNE this program will read the buffered IRM BPM data and/or the buffered Multiwire data as input for its tuning algorithm.

Another fixed target facility program which is being developed and needed by MiniBooNE as well as NUMI and the 120 GeV fixed target experiments is a fixed target ACNET data EXPORT program. This program reads ACNET spill data (BPM's, Multiwires, SWIC's, magnet currents, etc.), time stamps the data, and sends the data to the various experiment's Data Acquisition systems via ethernet. For MiniBooNE this program will read the buffered IRM data, the buffered SWIC system data, and other non time critical ACNET data during non beam pulses and send this data to the experiment's DAQ system.

2.4 Safety Interlocks (WBS 1.1.11)

A Safety Interlock System is required to prevent individuals from entering the enclosure while the beam is present. All requirements for personnel safety interlock systems (electrical and radiation) are stated in the Fermilab Radiological Control Manual (FRCM) [16], and the Fermilab Environmental Safety & Health Manual [17].

Critical devices are used to protect individuals from accidental exposure when entering the enclosures during periods when beam is present in the accelerator or in other remote areas. A critical device must have redundancy - that is, that at least two critical beam elements are turned off upon access to an enclosure. For the 8 GeV beam transport to MiniBooNE, the first critical device is the set of two dipoles at 862 that bend the kicked beam into the 24" berm-pipe under MI-10. These magnets must be energized to send beam into the 8 GeV line. The second critical device is a refurbished beam stop from the Meson Area.

Poly-bead bags are used around the outside of the beam pipe inside the 24" berm pipe for neutron shielding. Either of the critical devices is sufficient to keep beam from entering the 8 GeV Beam tunnel to

MiniBooNE. Hence, this set of critical elements is more than sufficient to protect individuals upon entry to the enclosure or the Target Hall.

The interlock system will require that the controlling power supplies are not only set to zero current, but actually turned off to allow entry. Controls for the safety interlocks will be housed in the MI-10 and Target Service Buildings.

DRAFT

Chapter 3

The MiniBooNE Neutrino Beam (WBS 2)

Conceptually, the neutrino beam consists of four sections (Fig. 3.1): the target, the focusing system, the decay region, and the beam absorber. These elements sit in the target hall (MI-12) and decay pipe. Fig. 3.2 shows the location of the target hall with respect to the 8 GeV beamline. The sections of this chapter describe the MI-12 building design and the beam technical elements.

3.1 Target Hall (WBS 2.3.1)

The Target Hall design for the MiniBooNE Neutrino Beam has evolved after extensive discussions and design work by the Beams Division Mechanical Support Department. The majority of the floor of the MI-12 building is open hatch. This allows fabrication of the target pile after the civil construction is complete, and hence provides the earliest beneficial occupancy of the building and enclosures. The target pile will be constructed first, while simultaneously being able to deliver components for the 8 GeV installation activities. Once the target pile is complete, the 24' long shielding blocks will be placed over the target pile, onto which technical equipment (in particular the horn power supply) can be installed. The section of 18'-long concrete blocks will be installed only after all of the components have been installed in the enclosures; in general, equipment will not be placed on top of the 18' blocks, since these blocks will need to be removed to bring any equipment into the enclosures, other than what can be carried down the stairs. Adjacent parking areas and a gravel hardstand will be accessible from Indian Creek Road. A stairway connects the MI-12 Service Building to the lower level where the target and horn are located within the Target Pile. A 1500 kVA transformer is located outside the building, and a ductbank brings power and communications to MI-12. ICW is provided for fire protection.

3.2 Shielding, Decay Pipe, and Absorbers (WBS 2.1.9)

Passive shielding and absorbers are used in the MiniBooNE Target Hall in order to contain the particles and maintain low radiation levels. Radiation issues are considered in detail in Chapter 5 of this TDR. Here we describe the components.

3.2.1 Beam Absorber Design (WBS 2.1.7, 2.1.9)

A highly divergent hadron beam exits the horn and enters the decay region. This beam consists mainly of unscattered and scattered primary protons and mesons. Quite unlike the high energy beams to which we

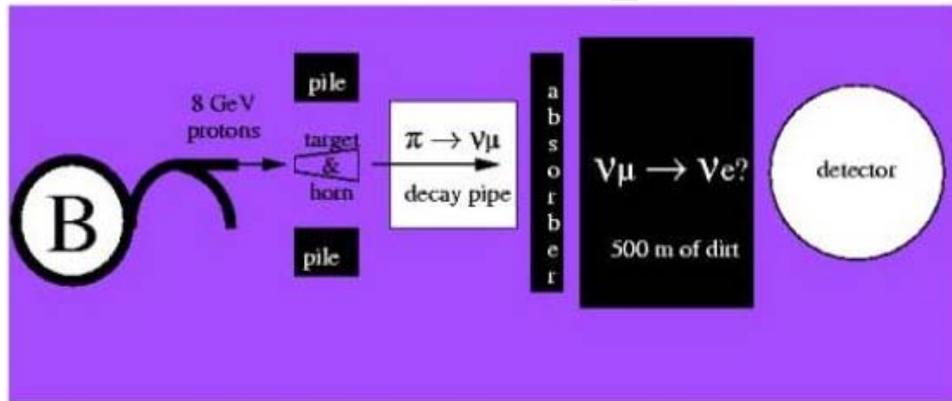


Figure 3.1: An overview of the MiniBooNE Projects showing the portion described in Chapter 3 by the shaded area.

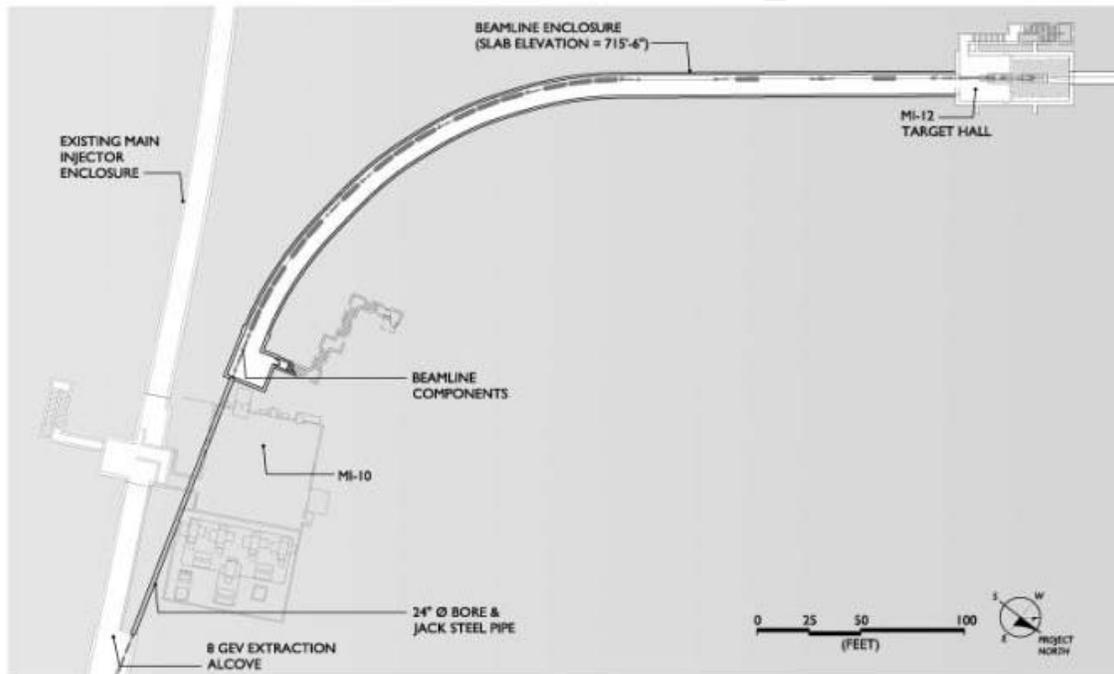


Figure 3.2: Below-grade plan view of the 8 GeV beam tunnel. Enlarged versions available in reference [5].

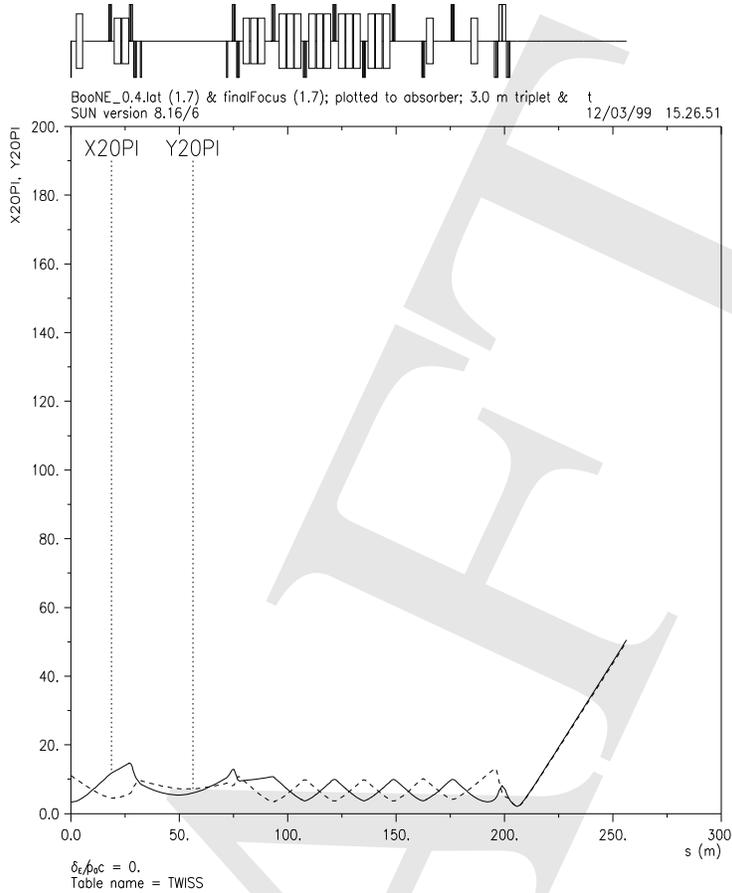


Figure 3.3: Beam profiles showing the growth in size as the 8 GeV proton beam drifts through the Decay Pipe for a 20π beam.

are accustomed at Fermilab, the proton beam is 100-150 mm wide at 50 m from the target (see Figs. 3.3 and 3.4). The pion beam is even larger. This large divergence was an important consideration for the decay region and absorber designs. At the end of the decay pipe, 50 m from the target, is a beam absorber which stops all the hadrons and low-energy muons. Located at 25 m from the target is an intermediate absorber which can be lowered into the beam. This design feature was introduced to provide a test of signal versus background, as described in Sec. 1.3.

The “50 m absorber” will be permanently located at the downstream end of the Decay Pipe. It has been fabricated from “blue blocks”; these blocks are being obtained from an outside vendor for use both by MiniBooNE and by NuMI. They are approximately 52” x 52” x 26” (weight approx. 10 tons) and have convenient lifting fixtures. Twenty-eight are required for the 50-m absorber. The absorber was installed in October 2000.

The “25-m absorber” is designed so that it can be lowered into the beam. It will be constructed from the Lab E detector steel, 10’ x 10’ x 2” plates (Fig. 3.5). These plates will be assembled into modules 1’ thick, weighing approximately 25 tons. One module will be placed permanently in a horizontal position, with its top surface just below the bottom of the decay pipe. The remaining modules will be suspended from above. The beam absorber will become one of the most radioactive elements in the beam because it absorbs most of the beam power. MARS [18] and CASIM [19] runs predict that residual activity, even after

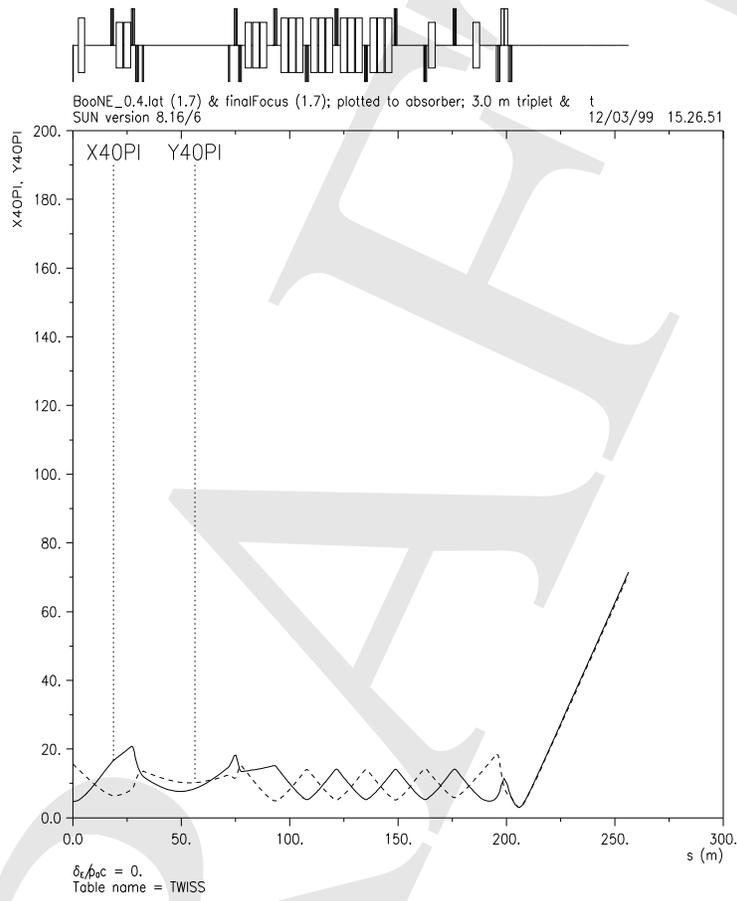


Figure 3.4: Beam profiles showing the growth in size as the 8 GeV proton beam drifts through the Decay Pipe for a 40π beam.

a week's cooldown, will exceed 100R/hr at the front face of the absorber. The absorber must therefore be built in a way that precludes exposure of workers to these "hot" areas. This has led to a "silo" design for the 25-m absorber region, as shown in Figs. 3.6 and 3.7. Figure 3.8 shows a schematic diagram of the 25-m beam absorber. It is expected that the 25-m beam absorber will be in the beam for only a brief 4-month run. The absorber requires a certain minimal amount of cooling when sitting in the beam. The beam power into the steel is approximately 10 kW. Likewise, the volume of soil around the decay pipe also needs cooling. A network of air ducts will circulate air in this region, removing the heat both from the soil and the absorbers. This air is circulated in a closed system, exchanging its heat with the outside air.

An array of 24 monitors will be embedded near the back of each absorber. They will be placed deep enough into the absorber that only the highest energy muons (greater than 3 GeV) will survive. The monitors that have been chosen for this are modified Tevatron Beam Loss Monitors (ionization chambers.) The modifications are to make them more radiation resistant, and to provide independent high voltage feeds rather than daisy-chained. In order to provide a cleaner signal from the monitors, they have been placed after about eight feet of steel to range out most hadrons. An additional three-foot layer of concrete then attenuates the neutrons.

3.2.2 Little Muon Counters

An additional device for measuring the secondary beam composition will be installed in the absorber region. The Little Muon Counters (LMC) will use a tungsten-scintillator range stack to measure the momentum distribution of muons emerging from the secondary beam at an angle of 7° . This will allow muons from K decay, which have transverse momentum up to $p_T \sim 236 \text{ MeV}/c$, to be distinguished from π -decay muons which have $p_T \leq 30 \text{ MeV}/c$.

The LMC system consists of a muon drift pipe which intersects the main decay pipe at a position 9 m upstream of the 50 m absorber. The drift pipe is steel, 8" in diameter, and will be filled with helium. The pipe is 55 feet long and passes near the eastern edge of the 50 m absorber; the pipe terminates in a 14 foot diameter steel vault which will sit below grade. A collimator and the range stack detector will reside in this vault.

The LMC components are being procured and installed using funds from outside the MiniBooNE project and will be described in detail in a future design report.

3.2.3 Target Pile (WBS 2.1.8)

Figure 3.9 shows an elevation view of the target pile. This view includes the stripline, horn, collimator, and surrounding steel shielding. Not included are the 18" thick concrete shielding blocks on the top, front, and sides of the pile. Figure 3.10 shows the stripline extending upward toward the Target Service Building.

Radiation shielding in the Target Hall requires about 6 feet of steel between the secondary beam centerline and the outside edge of the target pile. The bulk of this steel will be the "blue blocks" described earlier. The pile provides adequate shielding to contain the showering of radionuclides and keep their concentrations at the aquifer below EPA and DOE limits during normal and accidental loss scenarios. This is discussed further in Chapter 5.

The target pile provides a cavity into which the horn is inserted from the upstream end. The horn is contained within an air-tight box (Fig. 3.11), with the following connections: (i) Two horn striplines, discussed in more detail below, each consisting of five aluminum plates separated by ceramic spacers, cooled by a closed-loop air cooling system. (ii) Water supply and return for the horn cooling system. (iii) The beampipe/target assembly, consisting of the beampipe, four beam position monitors, a titanium vacuum window, and the beryllium target assembly, which is cooled by a closed, high-pressure air or nitrogen system. The box containing the horn has alignment fiducials and mounting feet. The mounting feet mate with the appropriate features on the "adjuster module." The adjuster module has jack screws for elevation adjustment, and rack and pinion drives for horizontal adjustment.

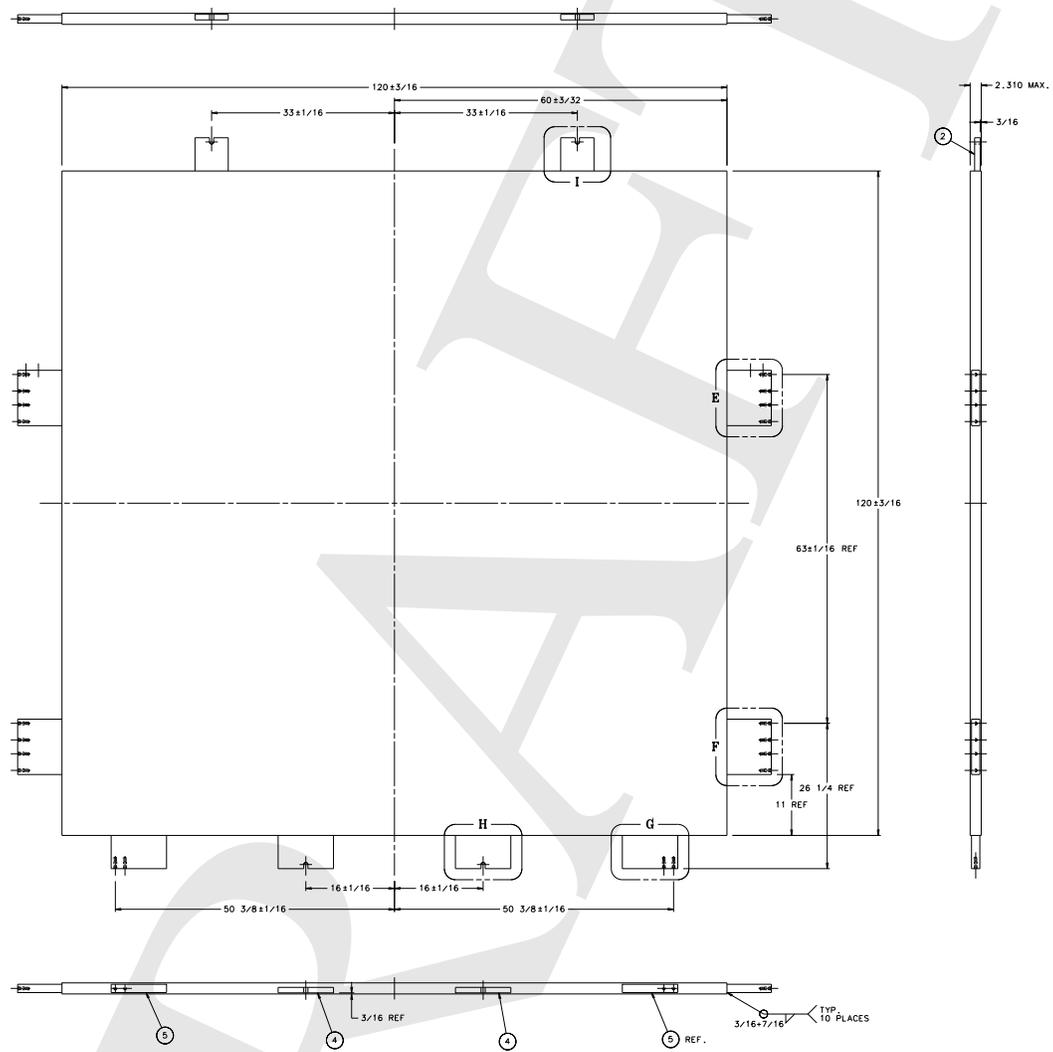


Figure 3.5: A schematic diagram of the Lab E steel plates that will be used for the 25 m beam absorber. Protrusions will be removed.

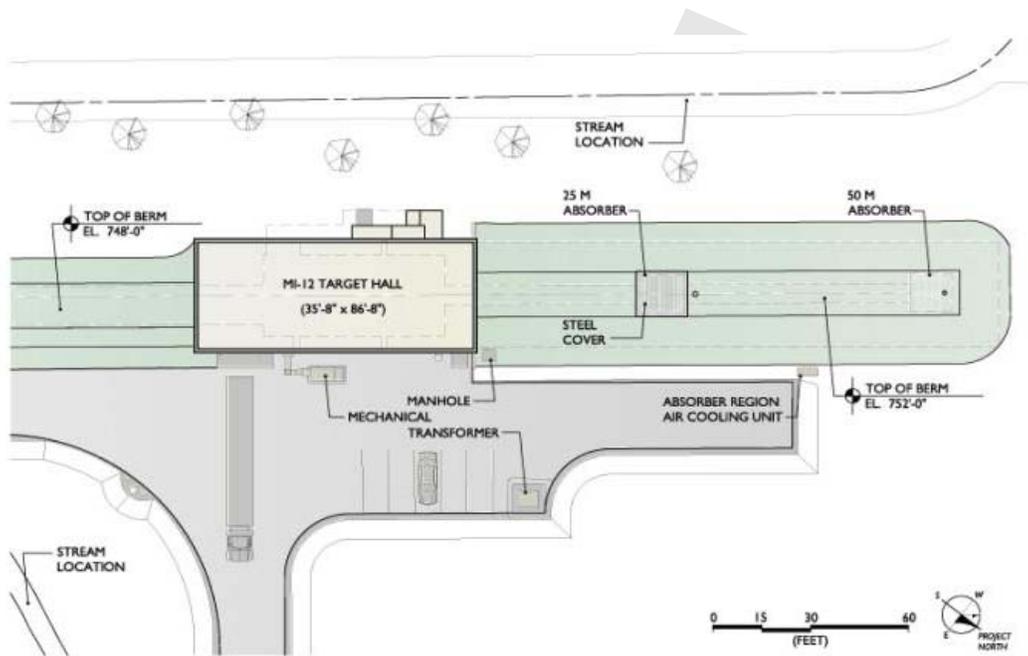


Figure 3.6: Above-grade plan view of the Target Hall, decay pipe and absorbers. Enlarged versions available in reference [5].

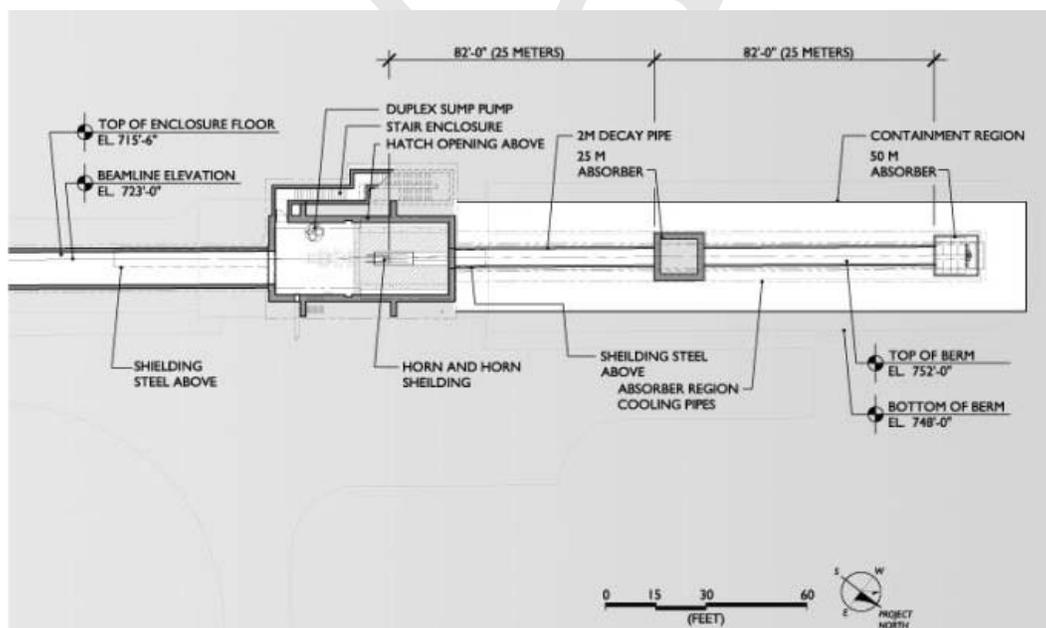


Figure 3.7: Below-grade plan view of the Target Hall, decay pipe and absorbers. Enlarged versions available in reference [5].

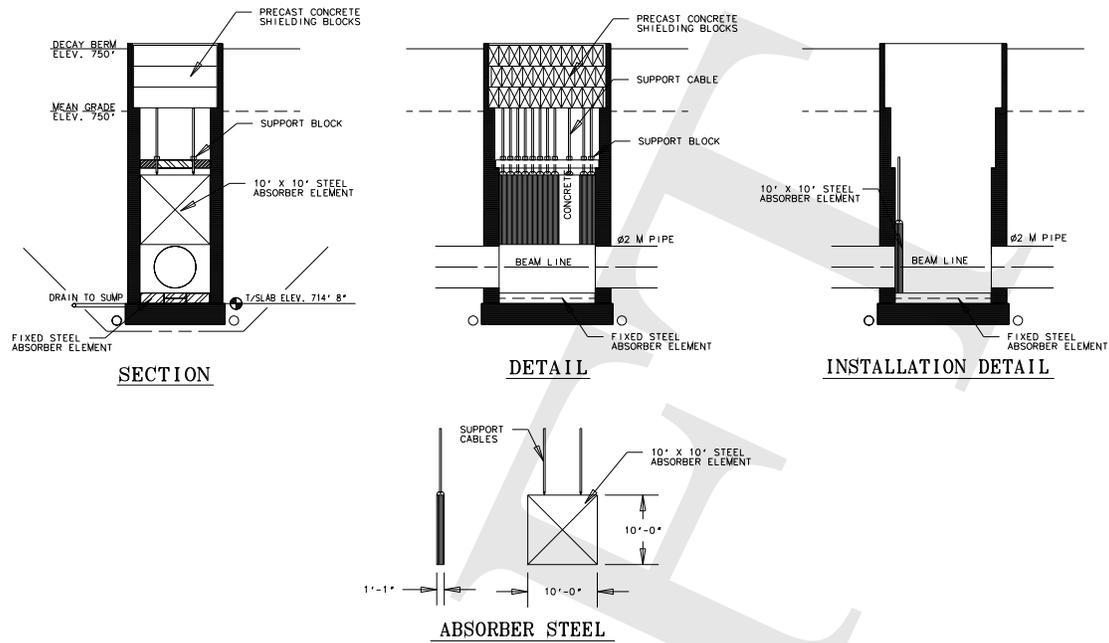


Figure 3.8: Sections showing the 25m absorber silo and the installation process.

A “shutter” mechanism at the upstream end of the target pile allows for horizontal retraction of 32 inch thick shielding doors for accessing the horn module during hot horn changes. Only the stripline and beam tube region remains open during running.

General Target Pile Assembly

The target pile requires approximately 160 “blue blocks,” (1600 tons), 60 concrete shielding blocks (300 tons) and special custom sized steel (40 tons) above and below the horn module. LCW cooled stainless steel panels will be installed on the top and sides for convective cooling of the pile. In addition, the top and front of the pile will have a sheet metal air shield installed and sealed to the concrete enclosure to minimize the amount of activated air leaving the target pile region.

The construction schedule assumes that the assembly of the pile will be done after the completion of the conventional construction activities. The target pile assembly will be done concurrently with the installation activities of the components into the adjacent 8 GeV line. This will require some interleaving of the crane usage to permit the 8 GeV line installation to proceed as rapidly as possible, since those activities appear closer to the critical path.

Collimator Attached to the Target Pile

A collimator sits immediately downstream of the Target Pile, and is nominally part of the Target Pile. The purpose of this device is to stop hadrons that would hit the enclosure wall rather than entering the Decay Pipe. The collimator shape is flared, with the small opening upstream and the large opening downstream. One must keep in mind that hadron production at 8 GeV is much more spherical than typical of higher energy FNAL experiments. So at MiniBooNE, such a cone (actually, a frustum) is important. The result is that the hot region from the wide angle particles is within the collimator rather than in the Decay Pipe. If the design were cylindrical rather than conical, the downstream lip of the collimator would become extremely

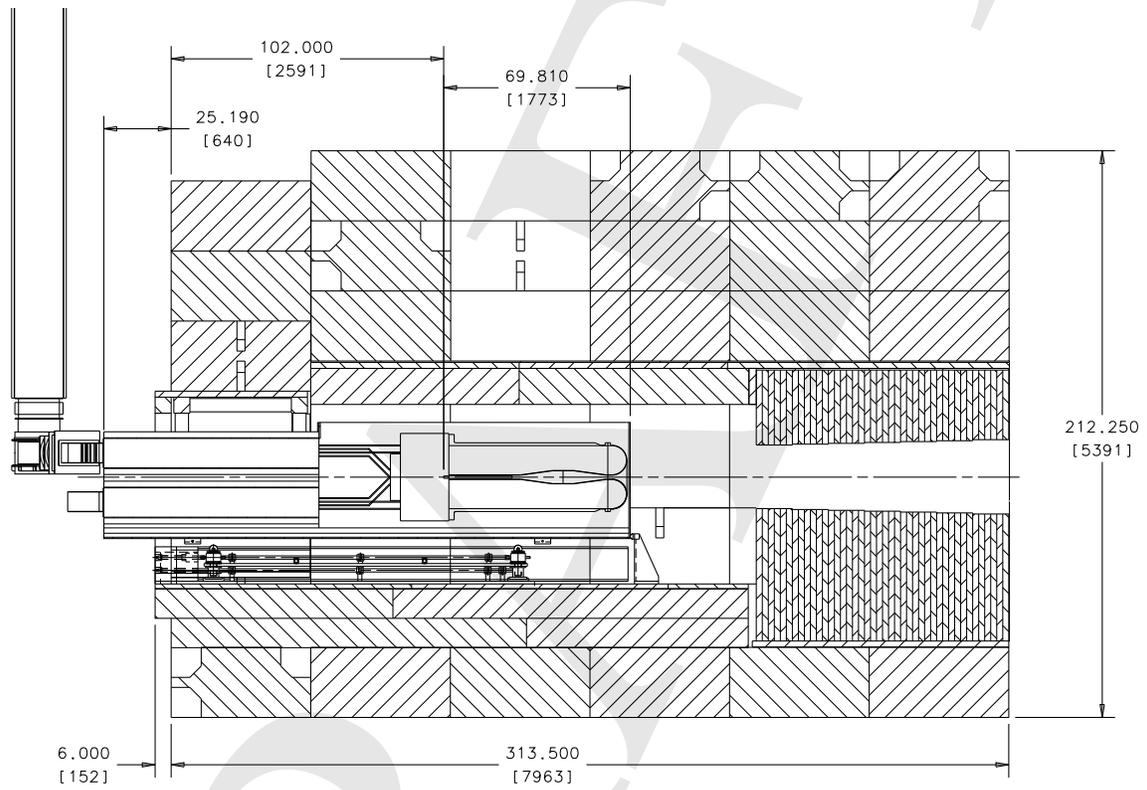


Figure 3.9: An elevation view of the target pile, including the horn, adjuster module, shielding steel. The stripline extends upward at the left.

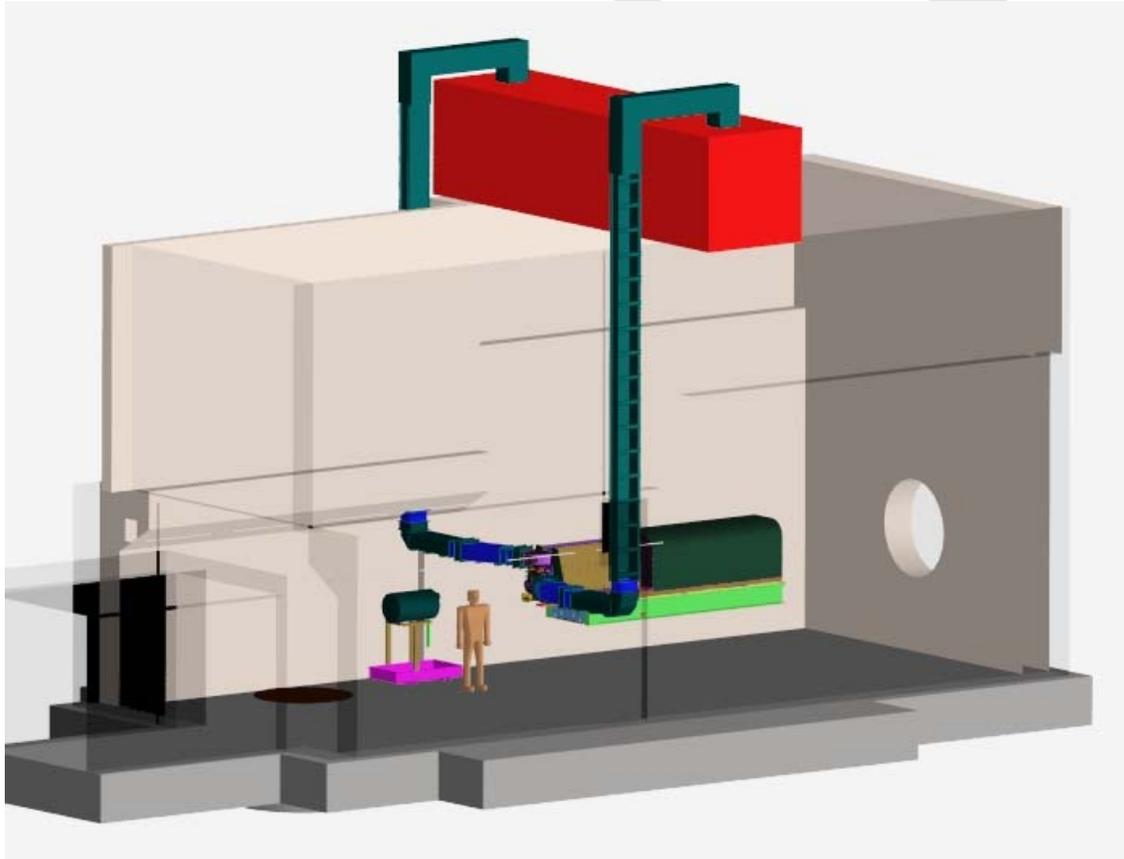


Figure 3.10: View showing the stripline coming down from the power supply in the surface building (building not shown), through vertical penetrations, and down to the horn in the shielding vault below ground. The concrete and steel shielding around the horn is not shown for clarity.

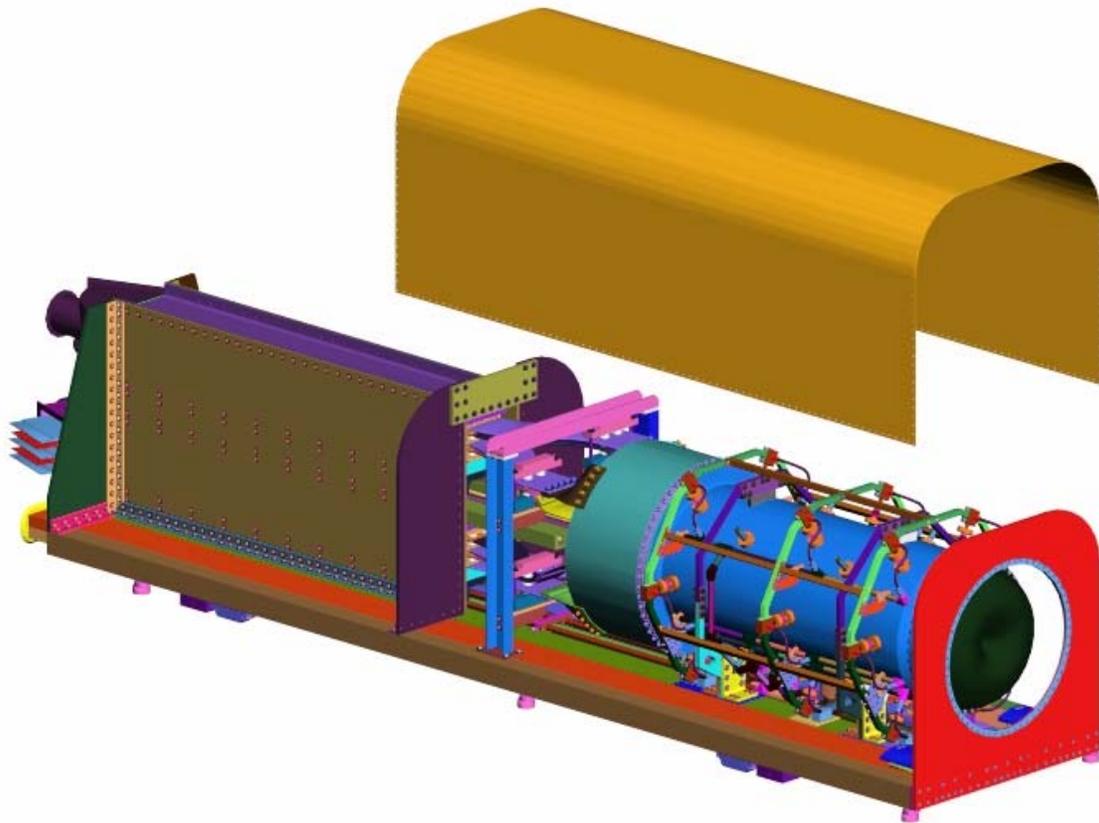


Figure 3.11: Horn in box with air-tightening cover suspended above. The thin Al downstream window is not shown so that the horn can be seen through the aperture.

hot, and additional shielding would be required beneath the service building. The collimator follows a ray from the inner radius of the decay pipe at $Z=25$ m drawn to the outer edge of the downstream end of the horn. This results in the following collimator dimensions. The upstream radius of the collimator is 30 cm at the distance of 259 cm from the target. It flares out to a radius of 35.5 cm at the downstream face, 473 cm from the target.

For ease of installation the collimator will be segmented into 7 modules (8 tons each) with each module made up of six 2" thick steel plates. A slightly stepped conical aperture will be formed by stacking the 2" thick plates with increasingly larger holes cut in them. The modules will be shimmed at installation for proper beam line alignment.

Horn Platform (WBS 2.1.12)

The lower portion of the pile provides a stable platform from which the target and horns can be aligned. A cavity exists within the Pile for the horn box. An adjuster module will be used to support and adjust the position of the horn box; the horn itself will have been previously referenced to fiducials on the outside of the box, which will be visible through channels in the bottom of the box. The alignment tolerance for the target and horn is 0.5mm.

The adjuster module rests within the target pile and supports the Horn Box at three points. These three support points are independently adjustable to provide movement up and down, side to side, pitch and yaw. Shafts pass through shield steel at the upstream end of the module to actuate radiation hard jacks and gear actuated metal slides under the horn box providing the movement.

The stripline from the power supply is connected to the stripline on the Horn Box with a clamped joint. Ceramic bars are alternately placed between the five conductors and clamped around the outside. Varying the amount of overlap of the machined tabs on the end of each conductor provides for length adjustability at each joint. Therefore the horn position can be adjusted with the adjuster module to match the beamline without moving the entire stripline.

3.3 Horn and Target (WBS 2.1)

Protons from the primary beam strike a 71 cm beryllium target, producing short lived hadrons with a typical transverse momentum of $0.3 \text{ GeV}/c$. The hadrons are focused by the magnetic fields generated from a high-current-carrying device called a "horn." The target is located within the magnetic focusing horn. A horn was chosen because it gives higher angular and momentum acceptances than other focusing systems. It can be made to withstand high radiation levels, has cylindrical symmetry, and also gives sign selection. Reversing the sign selection can provide a useful check of systematics.

A horn contains a toroidal magnetic field in the volume between two coaxial conductors. Current flows along the inner (small radius) conductor and back along the outer (large radius) conductor. There is no field inside the inner conductor, nor outside the outer conductor. In the volume between the inner and outer conductors, the magnitude of the field is given by $B(\text{kG}) = I(\text{kAmp})/5 \cdot R(\text{cm})$, and its direction is azimuthal (the field lines are toroidal, encircling the inner conductor). The inner conductor shape and current were optimized by using GEANT [20] to maximize the ν_μ flux between 0.5-1 GeV at the detector while minimizing flux above 1 GeV. The horn was optimized to run at 170 kA. While it may take running at higher current, the fatigue life of the horn would almost certainly be diminished.

Because of the high cycle rate of the beam, many more protons/year will be delivered to MiniBooNE than to previous neutrino facilities. This presents technical challenges on many fronts: target heating and cooling along with their accompanying stresses, including in the thin-walled aluminum conductors of the horns; cooling and heat exchange of highly radioactive water; radiation damage to components; and the handling and repair of devices with much higher residual radiation levels.

Table 3.1: Properties of Aluminum Alloy 6061-T6.

Young's Modulus	1×10^7 psi
Density ρ	2.71 gm/cm^3
Melting Temperature (minimum)	600°C
Thermal Conductivity	$180 \text{ W/m-}^\circ\text{C}$
Specific Heat	$0.23 \text{ cal/gm-}^\circ\text{C}$
Coefficient of Expansion	$26 \times 10^{-6}/^\circ\text{C}$
Electrical Resistivity	$3.8 \times 10^{-8}\Omega\text{m}$
Poisson's Ratio	0.34
Tensile Strength(static)	45000 psi
Yield Strength(static)	40000 psi
Strength after 10^8 cycles	14000 psi

3.3.1 Horn specifics

The MiniBooNE horn system was designed by satisfying a number of requirements and constraints placed on the design. The primary requirement was to produce a magnetic field with the correct focusing characteristics to produce the desired pion beam. The magnetic field created the constraints on the geometric shape of the horn and the current pulse characteristics, leading to the time structure of the pulse and the tubular and conical shapes of the inner and outer conductors. The need to maximize the low energy flux necessitated the use of relatively thin, relatively low Z material. The constraint combination of cost, electrical conductivity and the need to minimize the residual radioactivation of the components lead to the choice of aluminum, Al 6061-T6 (See Table 3.1) for the horn and its support structure and stipline.

Another requirement on the horn was that it survive a maximum number of current pulse cycles to minimize the cost of building multiple horns. A design life of $1 - 2 \times 10^8$ cycles was chosen to keep the number of horns needed to do the experiment to two at the most. This constraint tends to drive the wall thickness on the horn to thicker values, while the flux and activation constraints tend to drive the wall thickness down. Many finite element analyses were performed to understand the behavior of the horn under the pounding of the current pulse. See sections 3.3.2 and 3.3.4.

The horn box was designed to satisfy the need to deliver utilities such as electrical current and cooling water to the horn, to provide air cooling for the stripline to the horn, to contain radioactive air inside the box for a minimum of four hours, and to allow the horn to be aligned to the beam-line. The horn box also allows precise assembly and disassembly of the target module and BPM/vacuum pipe module with the horn.

A rendering of the solid model of Horn MH1 is shown in Figure 3.12. The horn support platform and cover are rendered transparent in this image to see the internal structures. On the right side of the figure the cylindrical object is the horn. On the left is the stripline connection to the horn, enlarged in Fig. 3.13.

The horn has a total length of 73 inches (185.4 cm) and an inner conductor radius that varies from .87 inches (2.2 cm) to 2.58 inches (6.54 cm). The outer conductor is 23.62 inches ID (60.00 cm). The maximum magnetic field for 170 kA is 1.5 Tesla.

The detail on the upstream end of the horn of Figure 3.12, which is enlarged in Figure 3.14, shows the many pieces necessary to bolt the upstream end of the horn into a water-tight container, yet insulate the high voltage of the inner conductor from the grounded surface of the outer conductor. The intense radiation environment inside the horn box dictated that insulation be done entirely with non-organic materials. High purity Alumina ceramics separate the inner and outer conductors electrically. Aluminum metal seals were used as water gaskets in every connection.

Figure 3.15 shows the water supply and collection manifolds. The water exits through the 2 inch pipe along the bottom of the horn. For details on the unique aspects of the MiniBooNE cooling system, see section 3.3.3.

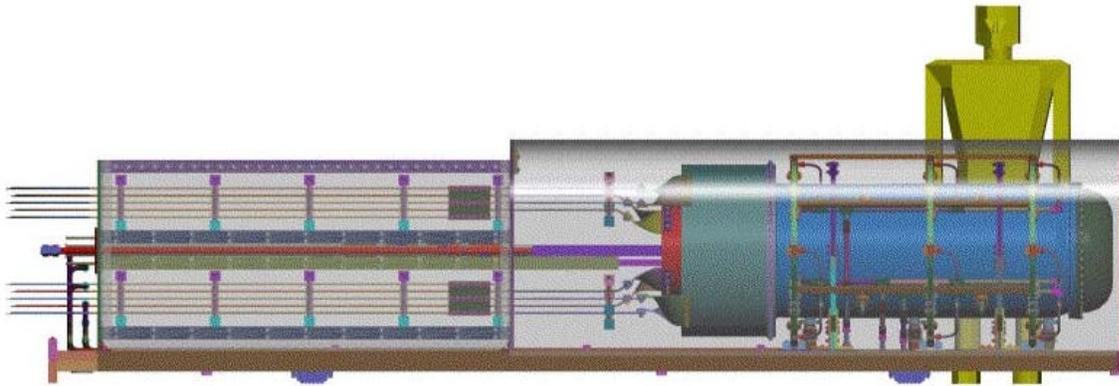


Figure 3.12: Side view of the horn, stripline and target with the horn box rendered transparent.

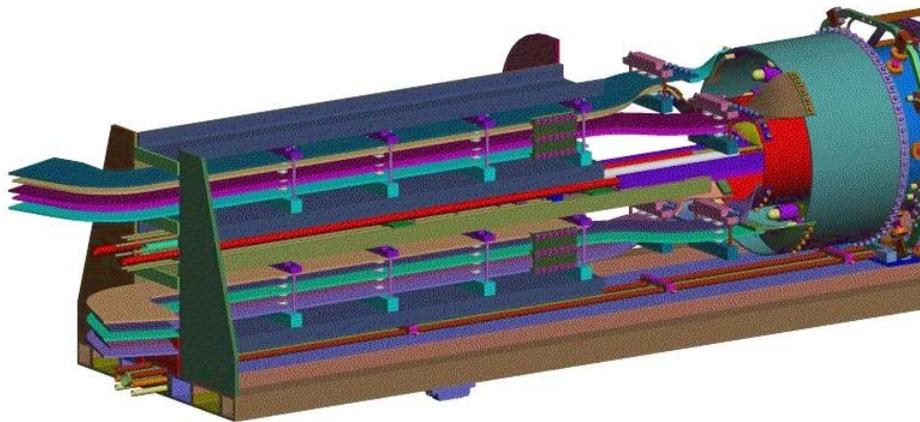


Figure 3.13: Stripline connection to the upstream end of the horn.

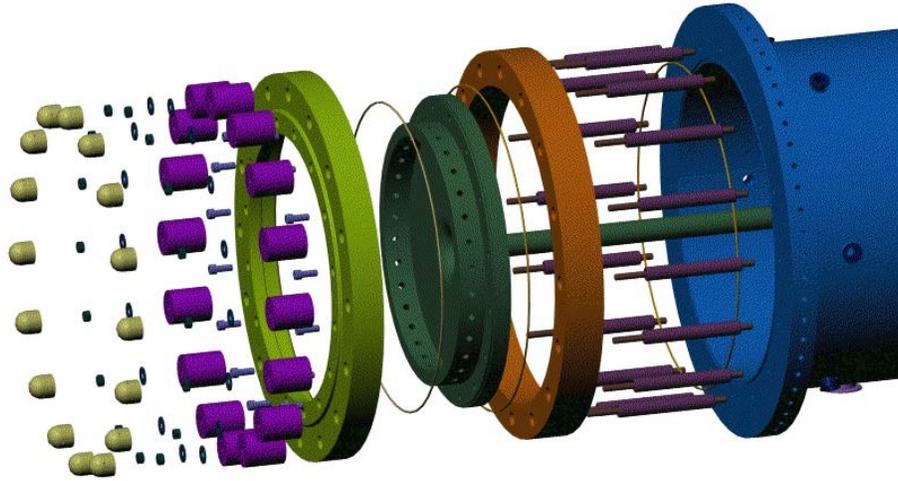


Figure 3.14: Exploded view of the upstream connection between the outer conductor, ceramic ring, and inner conductor.

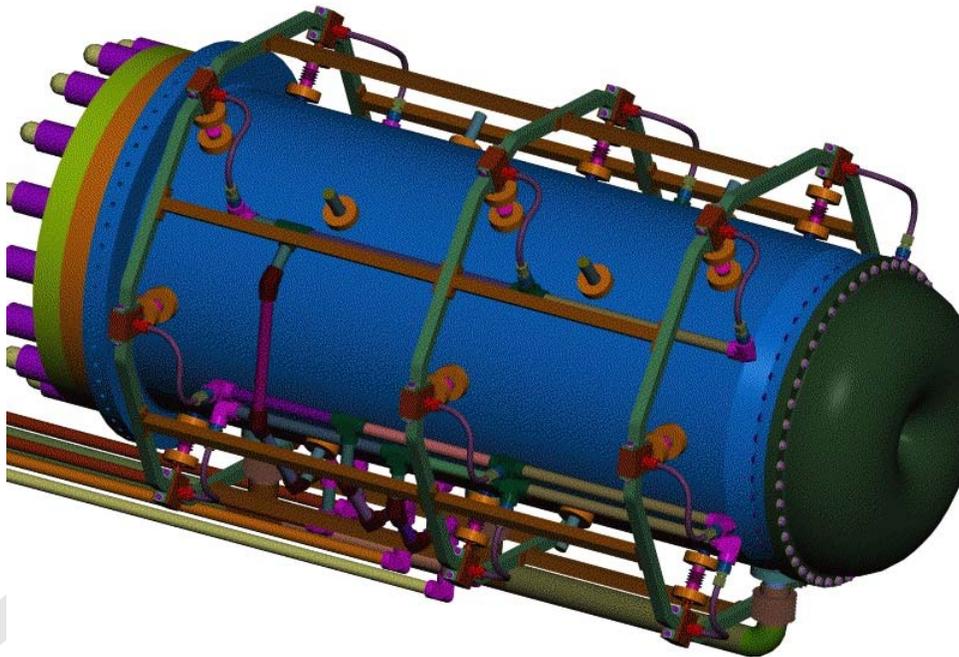


Figure 3.15: Outer view of the assembled horn and water truss.

3.3.2 The Finite Element Analyses of the Horn (WBS 2.1.4)

The design life of the horn is intended to be a minimum of 10^8 cycles. This lifetime is orders of magnitude beyond what has been achieved at FNAL previously, and longer than most horns built anywhere in the world have ever achieved. Aluminum does not have an endurance limit like steel does, so the determination of the maximum stress the horn will see was critical. Most fatigue data for aluminum provides maximum stress values for a 50% probability of failure at given numbers of cycles. As quoted in the table above, the usual maximum stress given for 10^9 cycles is 14 ksi. The horn had to be designed to a 97.5% confidence level for no failure at 10^8 cycles. The MIL-SPEC handbook contains a sample of Al 6061-T6 fatigue data presented as trend curves for maximum stress at 50% probability of failure as a function of the number of cycles, with different trend lines for different stress ratios (the minimum stress divided by the maximum stress in the cycle). This data also presented a mathematical model of the fatigue stress which could be used to present all of the test data on the same graph in a single trend line, the equivalent stress vs cycle life graph. The horn design team analyzed this data to generate confidence curves that showed that the maximum equivalent stress at 10^8 cycles had to be at or below 10 ksi everywhere in the horn to achieve the desired confidence. This graph is shown in Figure 3.16. With this equivalent stress, the maximum allowable stress was calculated accounting for such factors as notches, welding, exposure to moisture, and the stress ratio.

The finite element (FE) analysis progressed in phases. Previous work by NuMI indicated that a convective heat transfer coefficient at the surface of the inner conductor of about $3000 \text{ W/m}^2\text{K}$ was required to carry the heat of the inner conductor away. Testing on a pre-prototype by NuMI showed that this number was achievable in reality. The first FE analysis was a 2D axisymmetric transient thermal analysis using this heat transfer coefficient to see the effects in stress and deformation on the horn of the heat caused by the current pulse trains. This analysis allowed us to calculate the steady state average temperature of the horn, and the minimum stress state of the pulse cycle. We found that the time just before the next current pulse had no magnetic stresses and minimum thermal stresses.

ANSYS has the ability to calculate magnetic forces and stresses given current distributions, but this analysis requires a 3D model. This model became too large to do the combined thermal/magnetic analysis that we required, but it did allow us to qualify some analytical expressions that were derived from first principles for magnetic pressure. We verified the analytical expressions in the 3D model, and then used them to generate equivalent magnetic pressures in a 2D axisymmetric magnetic model. By making a 2D magnetic force model we could easily integrate the results of the thermal and magnetic analyses. The maximum stress state at every point in the 2D model was determined by combining the magnetic stresses at peak current with the thermal stresses at maximum temperature.

Ultimately, a large Excel spreadsheet was created that contained the principal normal stresses at every element in the horn model at both the minimum stress state and the maximum stress state. These numbers allowed the stress ratio to be calculated at every element in the model. Combining the stress ratio with other factors such as the reduction in maximum stress caused by welding on the material allowed the maximum allowable stress for fatigue to be calculated at every element. The principal normal stresses were then combined into a stress value that could be compared to the maximum allowable stress in fatigue. Finally, the calculated stress was divided by the allowable stress to get a ratio at every element in the model. It became trivial to spot where there might be trouble simply by determining whether this final number was greater than or equal to one. This is how the graph of Figure 3.17 was created. The spikes on this graph that go beyond 1.0 were discovered to be the thin wall at the welded connection between the downstream inner conductor cone and the end cap. This wall was thickened to bring every ratio of calculated to allowable stress below 1.0.

3.3.3 Cooling of the Horn (WBS 2.1.3, 2.1.10)

The finite element analysis started by assuming a heat transfer coefficient for spray cooling. Unfortunately, no way was determined on how to scale the NuMI heat transfer test data to the MiniBooNE geometry. It was decided to measure the heat transfer coefficient for MiniBooNE geometry in a test setup similar to

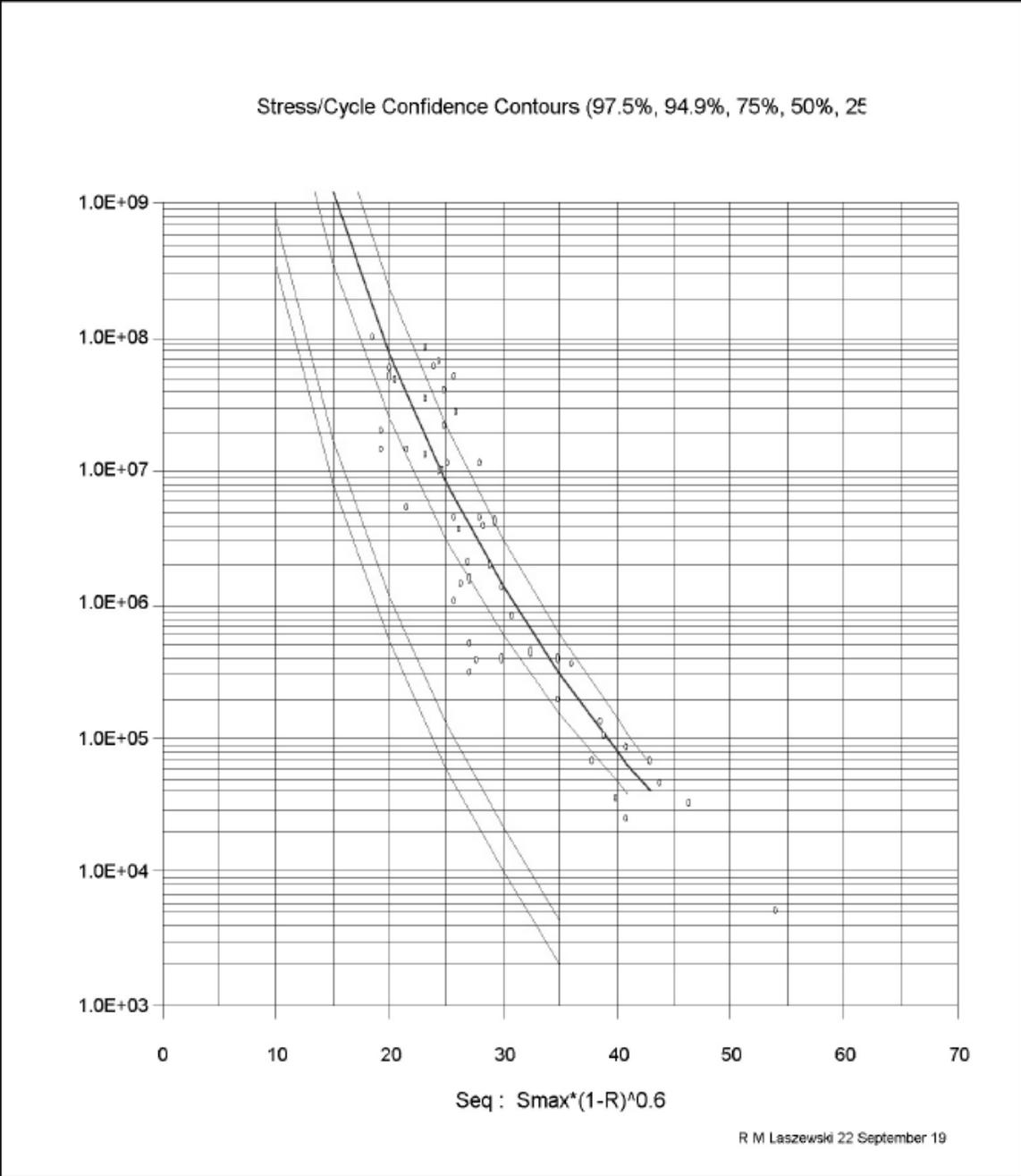


Figure 3.16: Graph of the number of cycles to failure for Al 6061-T6 vs equivalent stress in ksi. Different curves represent different confidence levels.

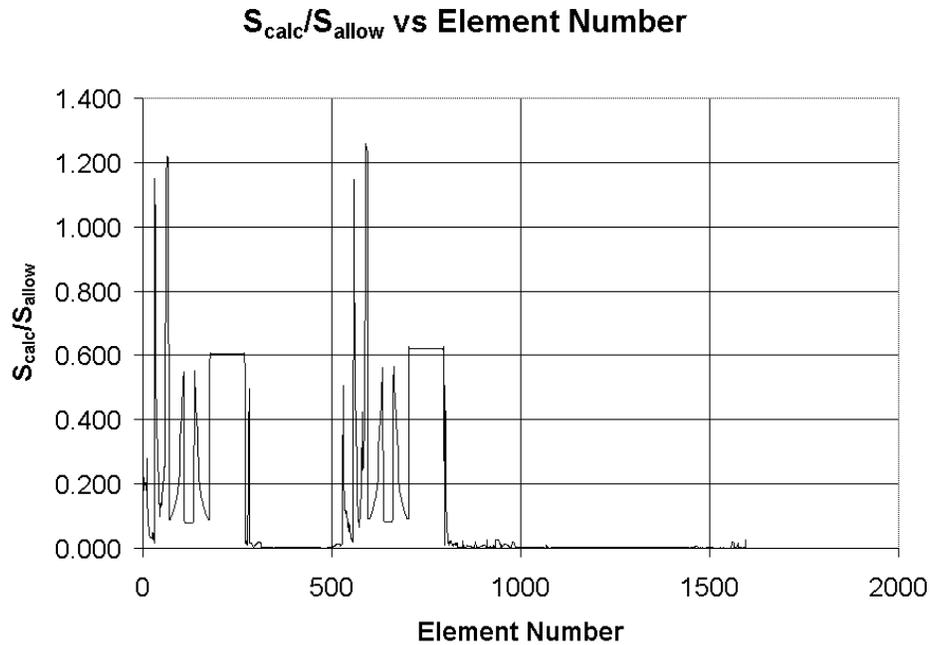


Figure 3.17: Graph of ratio of calculated stress to allowable stress vs element number.

NuMI's but sized for MiniBooNE. This section describes that experiment and the unique characteristics of the MiniBooNE water cooling system.

The horn design team studied the design of horns from around the world, past and present, and came to some conclusions about the design features of the MiniBooNE horn. In particular, the cooling system for this horn is a hybrid of the system developed for the NuMI horn with modifications inspired by the K2K and BNL horn cooling systems. In this section, we describe the experiment performed at the Proton Assembly building to determine the convective heat transfer coefficient we could expect with the size and shape of the MiniBooNE horn. We also describe the cooling system.

Determining the Convective Heat Transfer Coefficient in Droplet Spray Cooling

While it is theoretically possible to predict the heat transfer coefficient in droplet spray cooling, in practice it was almost impossible to find a mathematical model that could be used for our geometry in engineering textbooks and literature. It was our judgement that it would be cheaper and more reliable to build a small test stand to measure this critical parameter than it would be to hire a computational fluid dynamics consultant to calculate the coefficient.

The MiniBooNE test stand was designed along the same lines as the previous NuMI test, but with an outer conductor simulator twice as large in diameter. The basic concept was to spray water on an electrically heated tube that simulated the inner conductor. By measuring the current and voltage on the heater element one can calculate the heat energy input to the system. By measuring the bulk temperature of the cooling water and the surface temperature of the inner conductor, one can calculate the heat transfer coefficient from the relation $Q = hA(T_s - T_b)$. Q is the energy input from the heater, T_s is the surface temperature of the inner conductor, A is the area of the inner conductor, T_b is the bulk temperature of the cooling water and h is the average heat transfer coefficient.

The graph of Figure 3.18 was calculated by averaging the heat transfer coefficient that was determined for a range of input powers at constant water pressure and number of nozzles. It shows that for a range of

input power bracketing the power we expect to be deposited in the inner conductor, we get heat transfer coefficients at and above the necessary $3000 \text{ W/m}^2\text{K}$.

The Horn Cooling System

MiniBooNE drew on much of the design and testing effort of NuMI in the design of the cooling system for the horn. The basic concept is to use elliptical orifice nozzles, called *VeeJet* nozzles, which create a wide spray of water along the long axis of the orifice, but have a relatively narrow width in the opposite direction. These nozzles are oriented such that the wide axis of the spray is parallel to the inner conductor. This causes most of the water spray to strike the inner conductor only, and minimizes the number of nozzles necessary along the length of the inner conductor.

The fatigue failure of the K2K horn water piping system made obvious the effect of the pulsing of the horn on a water system that is rigidly coupled to the outer conductor. The most unique aspect of the MiniBooNE cooling system is that the spray nozzles are not rigidly coupled to the outer conductor at all, as they are in every other pressurized water horn cooling system. The nozzles are connected to the outer conductor by a stainless welded bellows, a vibration isolation concept that allows the horn to be water-tight, but they should be relatively isolated from the vibrations of the outer conductor. See Figure 3.19 for a view of a single nozzle and its bellows.

Because the connection to the outer conductor does not support the water nozzles and supply tubes, the entire water system has to be rigidly supported by a truss that surrounds the horn but does not touch it. The water truss is connected to the horn platform, but is electrically isolated from it by ceramic blocks. This is to prevent whatever potential difference exists on the outer conductor from shorting to the ground of the horn platform. Figures 3.20 and 3.15 show the truss and nozzle arrangement. The drain pipe is also connected to the horn through bellows to prevent differential thermal expansion between the outer conductor and the drain pipe from inducing stress in either object.

The RAW System (WBS 2.1.10)

The horn will be cooled by radioactive water (RAW). The RAW system has a rated capacity of 16KW. The normal operating pressure of this system is 50 to 55 psi with flow rates up to 50 gpm. As with all RAW systems only one main pump may run at a time. These systems have two Temperature readouts and one flow readout. These are analog readouts and may be processed by the main computer system. There are 13 status points available from these systems along with the three analog points, (0-10 vdc). These points will indicate if a pump is operating, if the flows are proper, the temperature is OK, or the surge tanks are at the proper level.

When the RAW pump is started the water is supplied from the surge tank on the RAW skid. After the pump the RAW water is passed through a water to water heat exchanger to remove the heat from the water in the system. After the heat exchanger the water is passed through a 50 gpm Full Flow 10-micron string filter, to remove particulate content in the RAW water. After the Full Flow Filter the system splits into two separate branches, the Deionizing Branch and the Horn Supply Branch. The RAW water supplied to the Horn will drain into the Surge/Accumulation Tank on the RAW skid. During the testing the water will drain into a lower Surge/Accumulation Tank below the horn being cooled and pumped back to the upper Surge/Accumulation Tank on the RAW skid.

Further details on the RAW system can be found in Ref. [21].

Stripline Cooling (WBS 2.1.4, 2.1.14)

The stripline will be encased in an enclosure or duct that allows the stripline to be air cooled. The side frames of this enclosure are made from aluminum C-channels that provide structural rigidity to the stripline which will facilitate stripline transport and handling and provide protection during use. 85% of the stripline used in the horn test at MI-8 will be reused at the target service building. Three forced air cooling systems will keep stripline temperatures under control. The cooling systems are comprised of a blower, an air filter,

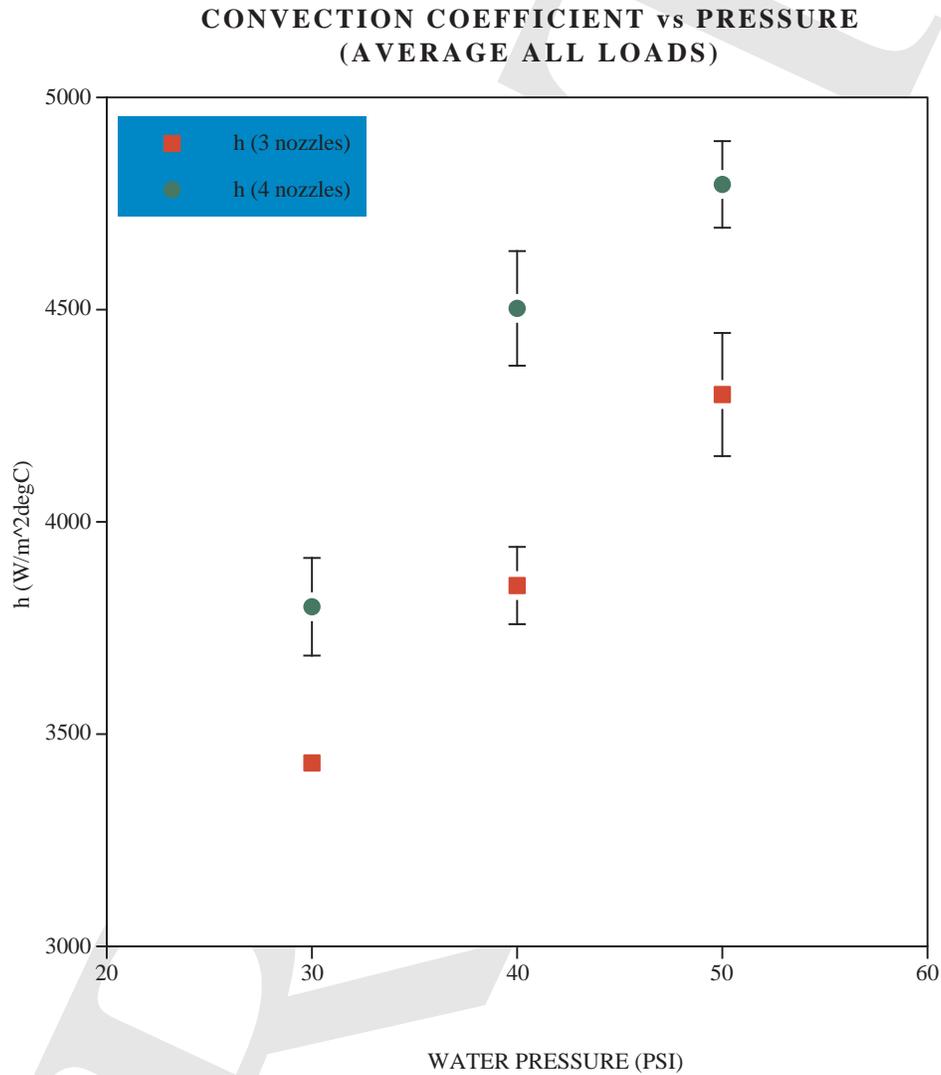


Figure 3.18: Graph of average heat transfer coefficient vs water pressure and number of spray nozzles in operation azimuthally.

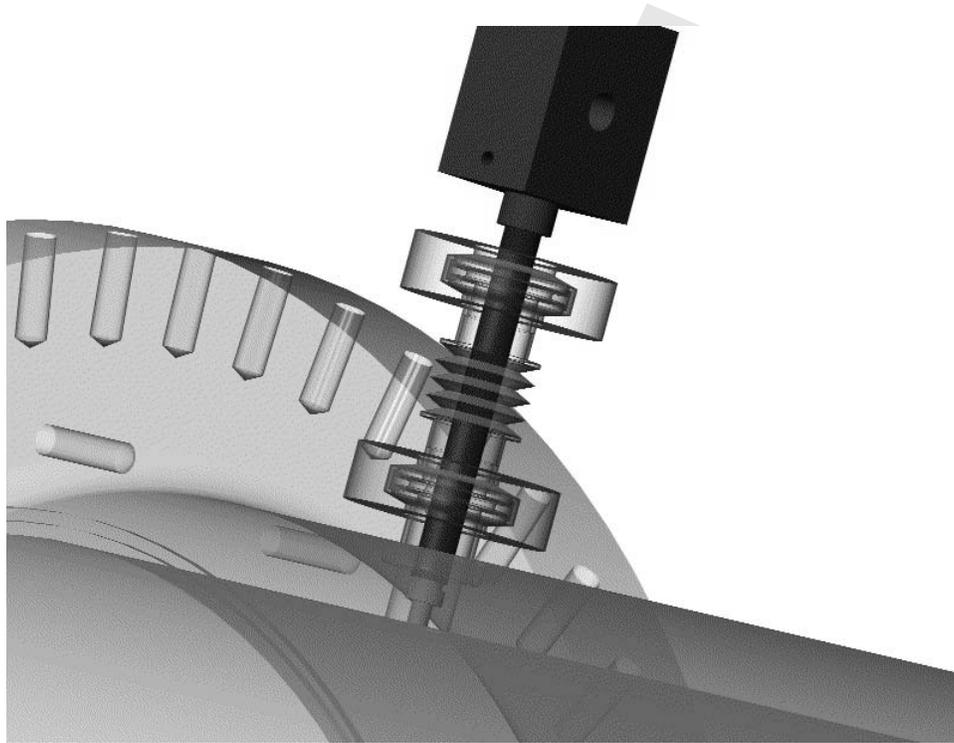


Figure 3.19: A view of a single spray nozzle with its vibration isolation bellows. The bellows and OC are transparent to see the nozzle tube.

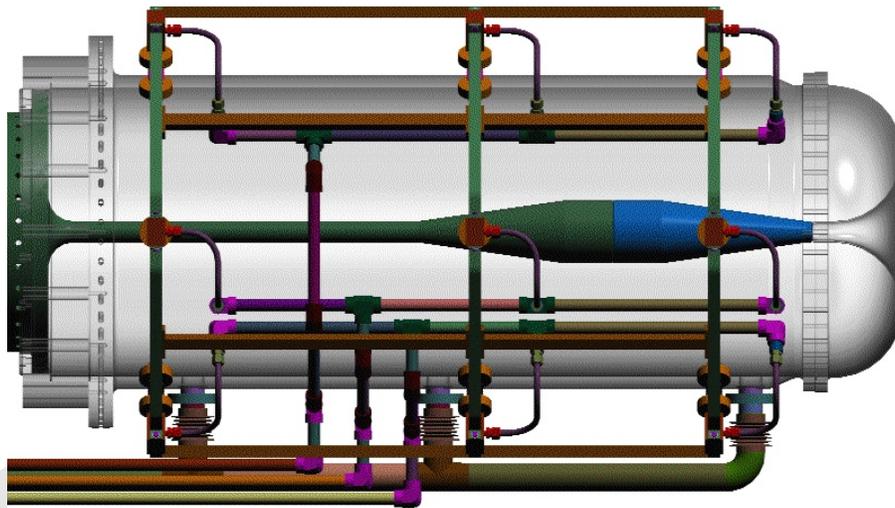


Figure 3.20: Side view of horn with the water system support truss. The outer conductor is rendered transparent here to see the spacing the of the cooling nozzles along the inner conductor.

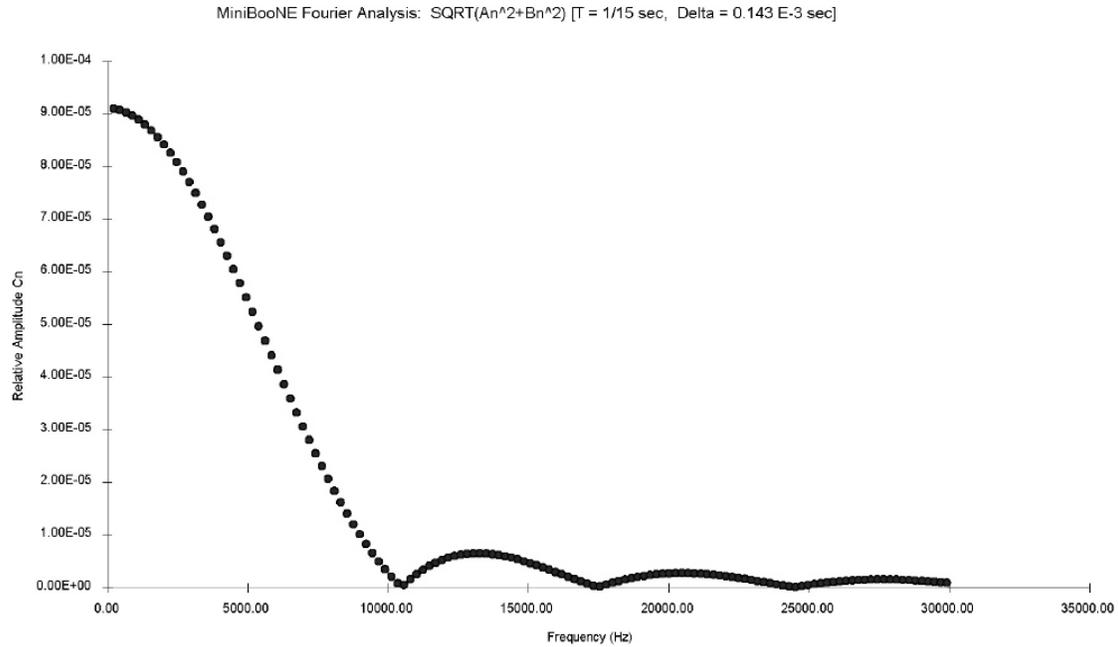


Figure 3.21: The Fourier spectrum of the MiniBooNE current pulse (ignoring the fine structure caused by the Booster cycle).

and a water cooled coil. The system that cools the stripline that passes through the radiation shield steel to the horn will be isolated from the other two systems to prevent the spread of radiation contaminated air.

3.3.4 The Modal Finite Element Analyses of the Horn and Fourier Analysis of the Vibration Power Spectrum (WBS 2.1.3)

The time structure of the current pulse on the MiniBooNE horn is a half sinusoid 143 microseconds long, repeated ten times in a row with 1/15 sec spacing between pulses. The horn then cools for about a second and a half before the next ten pulse train is initiated. This pattern of pulses was analyzed to see the Fourier spectrum of frequencies that could drive natural frequencies of the horn into resonance. If the mechanical Q of the horn is high enough, the pulse vibrations could excite resonances in the mechanical structure of the horn which could lead to deflections and stresses that would invalidate the structural finite element analysis of the horn. Another concern is that there could be a pulse scale factor associated with each current pulse, such that the horn might see some number of mechanical pulses for each current pulse. This would have the effect of scaling back the life of the horn because the number of fatigue cycles would not be the same as the number of current pulses. For example, assuming that each current pulse induced ten mechanical vibration cycles in the horn, then the fatigue life of the horn would be reached at one tenth of the number of current pulses.

As can be seen from the graph in figure 3.21, there are significant power contributions to the spectrum out to 7.5 kHz. Eigenvalue extraction of the natural frequencies of the horn indicates that the fundamental mode of the inner conductor could be as low as 77 Hz. This number is sufficiently close to a multiple of 15 Hz to be of concern that the pulse trains could excite resonances in the inner conductor. See Figure 3.22 for the results of the finite element extraction of the modes and natural frequencies of the horn without spiders. At this point, the contribution to damping from the water spray is an unknown, but potentially significant factor.

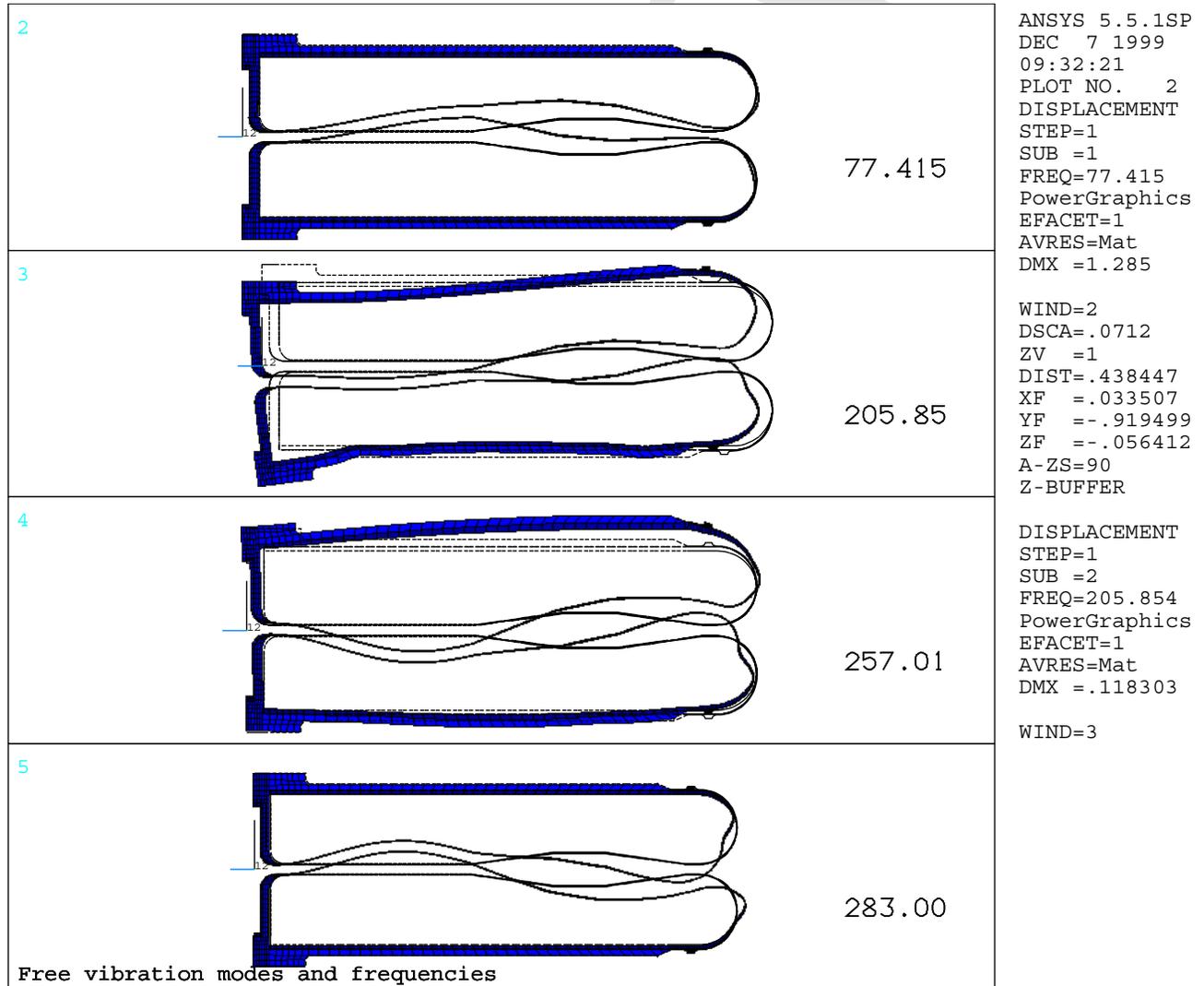


Figure 3.22: The first four modes and natural frequencies of the horn with no spiders. The amplitude is greatly exaggerated for illustration.

Table 3.2: Properties of beryllium

density	1.85 g/cm ³
interaction length	40.7 cm
specific energy loss (MIP)	1.59 MeV/cm
TCE	$1.2 \times 10^{-6} \text{ K}^{-1}$
specific heat	3.3 J/(cm ³ °K)
Young's Modulus	$3.1 \times 10^{11} \text{ GPa}$

When the finite element analysis of the horn was re-run with constraints between the inner and outer conductors (called “spiders”), the results showed that spiders could only practically raise the natural frequency of the horn to about 200 Hz, not enough to be out of the range of the power spectrum driving mechanical vibrations. Given that spiders did not look effective, it was decided to assemble and do initial testing of the horn without any spiders. Only if the results of the initial tests indicate that there would be significant large deflections of the inner conductor during pulsing would the horn be disassembled and spiders installed. The spiders that were designed for the horn would serve as a means of limiting the maximum deflection of the inner conductor and as an energy dissipation mechanism for the vibrational energy. Other means of absorbing energy have also been considered as modifications to the horn platform. These will only be implemented if testing indicates the need for such measures.

3.3.5 The Beryllium Target Assembly (WBS 2.1.5)

General Considerations

The beryllium target assembly serves to intercept the primary 8 GeV booster proton beam and to produce the primary interactions that yield secondary mesons that decay to neutrinos. It is thus a key element in the MiniBooNE neutrino production system. For the purposes of this design, the beam is assumed to have an emittance of 30π and a transverse sigma of 1.5 mm.

The MiniBooNE horn design centers around a target that is physically separated from the horn. That allows the target to be extracted without removing the horn itself, in the event of a target failure. Thus the target is entirely independent of the horn assembly and does not use the horn cooling system.

The choice of beryllium as a target material is based on the desire to: minimize the beam power load on the target cooling system, minimize the remnant radioactivity due to proton exposure, have a high pion production yield, and be resistant to material fatigue due to the large number of beam cycles expected at MiniBooNE. Some relevant properties of beryllium are shown in Table 3.2.

Radiological Properties

The target will potentially be exposed to greater than 10^{21} protons and thus poses a radiological hazard. This hazard has been reduced as much as possible by the choice of beryllium as the primary target material. In general, there are two radiologically important radio-isotopes produced in proton collisions on beryllium, ⁷Be and tritium.

⁷Be has a lifetime of 76.9 days and decays to ⁷Li via electron capture. The decay leaves the ⁷Li nucleus in the ground state 90% of the time, however, the remaining 10% of the decays leave the nucleus in the first excited state, which decays by emitting a 478 keV γ ray.

We expect a steady state asymptotic level of 15.7 Ci of ⁷Be in the target. That creates a 540 R/hr radiation level at the surface of the target. That level will be reduced to 10 mR/hr at a distance of one foot when placed in an appropriate shielded container (the current target coffin).

While the beam is on, activation in the gas coolant will cause a radiation level of around 10 mR/hr at a distance of 1 foot from the gas coolant piping. Within two hours of the beam being turned off, that level

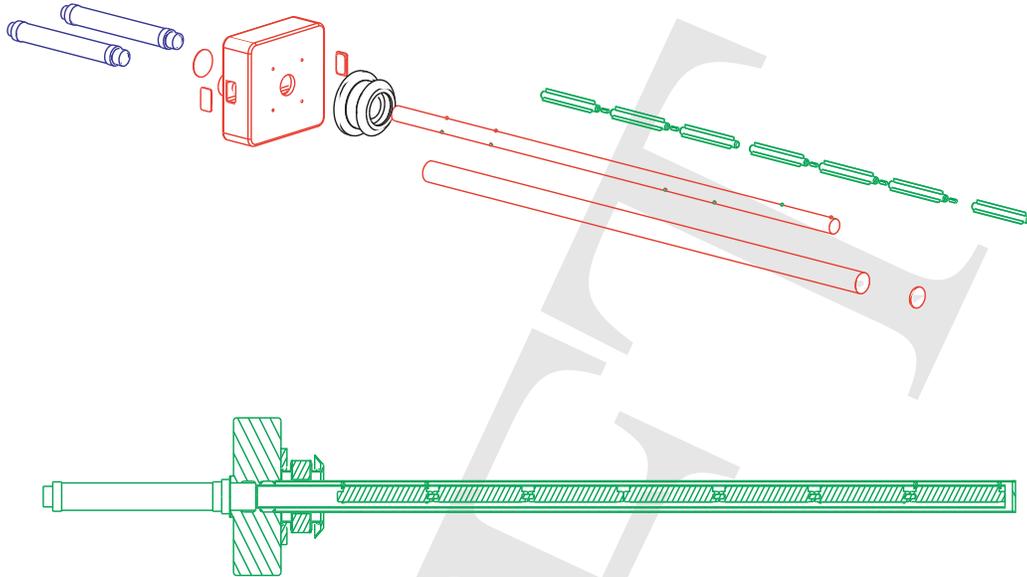


Figure 3.23: A drawing of the beryllium target assembly.

drops to less than 1 mR/hr.

Target Mechanics

The target consists of several mechanical units. The primary beryllium target elements, two concentric beryllium tubes, an aluminum manifold piece, and a stainless steel bellows that makes electrical contact with the horn inner conductor.

The primary target element consist of seven cylindrical slugs of beryllium. The slugs are four inches long and 1 cm in diameter with three radial cooling fins placed symmetrically around the axis. Dividing the target into short segments minimizes any forces on the assembly due to off-axis, asymmetrical heat loads from the primary proton beam.

The slugs are grouped into three upstream slugs and four downstream slugs. The slugs in each group are connected by asymmetric beryllium pins that prevent relative rotational motion between the slugs. Each slug-group is captured inside the inner beryllium tube by three titanium pin locators that capture the outer corner of the cooling fins. The locator and pin tolerances allow for thermal expansion and contraction of the target slugs.

The upstream end of the inner tube is electron-beam brazed into the aluminum manifold block. Its downstream end is left open in order to duct coolant gas back toward the aluminum manifold. The outer beryllium tube serves to support the inner tube, and to function as a duct for the target's gas coolant. The upstream end of the outer tube is electro-beam brazed to the aluminum manifold block, while the downstream end is capped by a beryllium endcap that is electron-beam brazed to the outer tube.

A stainless steel bellows is fastened to the manifold block in order to make electrical contact with the horn. This serves to prevent arcing between the horn and target assembly. The horn will rise to a few thousand volts during its pulse cycle and the target is in close proximity to it.

The aluminum manifold acts to provide a cantilevered support of the target-slug/tube assembly, to duct the gas coolant to and from that assembly, and to make electrical contact with the horn. It is machined from a solid block of aluminum. Four ceramic tube bolt assemblies support the manifold block onto the target fixture. They electrically insulate the entire target assembly from the horn and stripline support structure. The coolant gas connection is made via two ceramic tubes which have fittings brazed to them and screw into

Table 3.3: A breakdown of energy deposition sources in the beryllium target

Particle	Fraction	Power (W)
protons	0.78	475
pions	0.09	55
α and ^3He	0.10	60
D and T	0.03	17
electrons	0.01	5
total		611

the manifold block.

The instantaneous beam heating in the beryllium slugs could be of concern if the energy deposition were great. In the present case, the maximum temperature excursion will be about 6°K . With the beam profile in question, the resulting compressive pressures will be on the order of 20MPa. This is well way from published fatigue limit data on beryllium of around 300 MPa. Compressive waves propagate at around $13\text{ mm}/\mu\text{s}$ in beryllium. The transverse mechanical equilibration times will be on the order of the length of the booster pulse.

Target Cooling

The primary proton beam plus secondary particles deposit around 610 watts of power into the target slugs, assuming five booster pulses of 5×10^{12} protons per second. The calculation has been done several ways which all give similar answers. Table 3.3 gives a breakdown of the particles responsible as predicted by a GEANT/FLUKA simulation.

The beam heat load is removed by flowing air longitudinally along the beryllium slugs. We have measured the thermal properties of this arrangement in a prototype assembly, constructed of aluminum, and find it to be satisfactory. The properties agree with expectations derived from expected film coefficients for forced air cooling in standard engineering references.

A 700 watt cylindrical electrical heating element was inserted inside a finned, hollow aluminum extrusion to replicate the geometry and heat load of the beryllium slugs. The extrusion was inserted into two concentric aluminum tubes of the same size as the final beryllium tubes, and the assembly was connected to a manifold block of the same design as the final target. Air was blown through feed pipes by a 1200 watt fan motor which achieved a flow rate through the system of over 10 l/s. A final temperature rise of 130°C was observed on surface of the extrusion. That is sufficient for our purposes.

The gas system will operate as a closed loop. The external fan motors will be placed in a sealed box or housing. Gas will be delivered and returned via a pipes to the inner target pile. Filters will be located on these lines to inhibit radioactive, particulate material from contaminating the fan motor housing. Two fan motors will run in parallel to make the system more fault tolerant.

The temperature and pressure of the supply and return gases will be monitored in order to insure proper operation of the system. Any excursion from a steady state would be a sign of difficulty. Flow sensors will also monitor the presence of airflow on the supply and return sides. These will be interlocked to the beam delivery system. The temperature rise in the absense of cooling will be around 1.2°K per second. This leaves a reasonable amount of time for interlock systems to shut off the beam in the event of a cooling failure.

3.3.6 The Target Support Interface (WBS 2.1.6)

The target being provided by LANL is a set of beryllium slugs encased in tubes of beryllium which route cooling air around the slugs. The cooling air is directed to the target through the gas distribution flange at the upstream end of the target. This flange also mechanically supports the target from a structure that

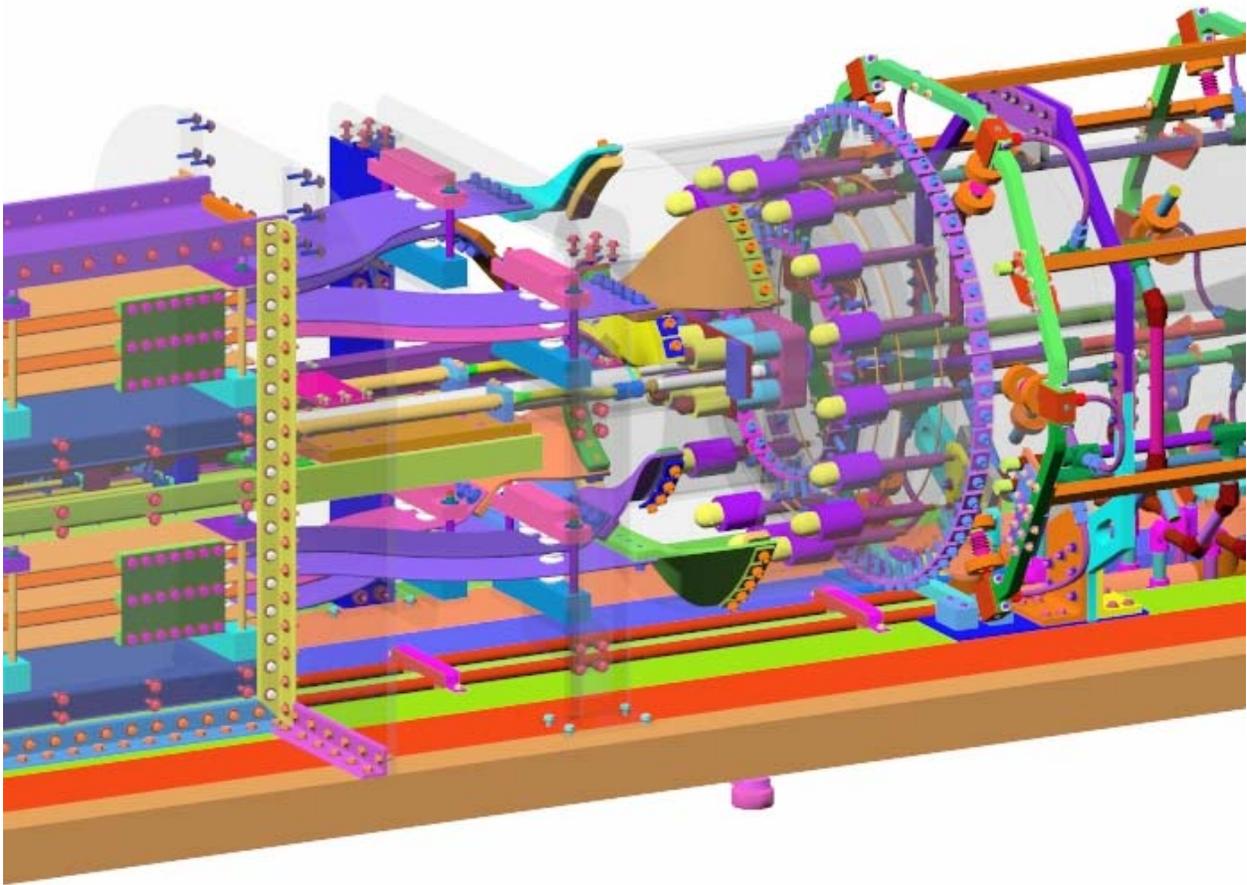


Figure 3.24: Stripline and beam pipe upstream of horn. The OC, IC and portions of the hornbox are rendered transparent to see the target insertion inside the horn.

allows the target to slide along rails inside the upstream end of the horn box, in between the upper and lower striplines. The target is inserted into the upstream end of the horn and fills most of the length of the upstream tube of the inner conductor. The target can be seen inside the transparent inner conductor of Figure 3.24.

The target support system was designed to minimize the complexity of alignment by using machined features in critical locations. If the target needs to be moved to align it to the central axis of the horn, these machined surfaces may be shimmed. The air tubing is supported by a pair of aluminum C-channels that provide bending support for the tubes, and longitudinal stiffness to push the target assembly into the horn box.

As is the case with the insulation between the inner and outer conductors of the horn, the target is electrically isolated from its support by ceramic tubes. It is also isolated from its air supply tubes by ceramic break tubes immediately upstream of the target gas distribution flange. A stainless flex hose protects the ceramic tubes from strain.

The same parallel Thomson rails that support the target module also support the vacuum pipe and BPM module. The rails are hidden inside the middle C-channel that supports the target in Figure 3.24. You can see the downstream end of the vacuum pipe with the thin titanium foil at the end in figure 3.25. This system

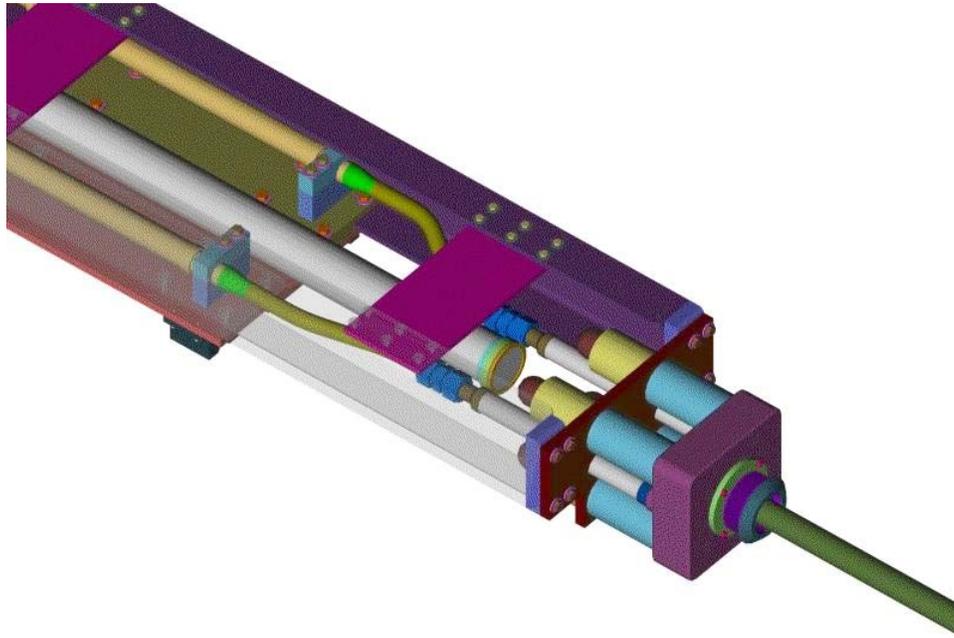


Figure 3.25: Close-up of the ceramic tubes and breaks that support the target and electrically isolate it from the support structure and incoming air cooling tubes.

maintains the aligned relation between the target and its beam position monitors, the cans in the middle of the beam pipe with cables coming off shown in Figure 3.26.

3.3.7 Horn Power Supply (WBS 2.1.11)

The power supply for the focusing horn is of the direct coupled design. Energy is stored in a capacitor bank and switched via a parallel array of sixteen silicon controlled rectifier (SCR) switches into the horn load. A parallel strip transmission line is used to connect the power supply to the focusing horn. The horn requires a train of pulses with a repetition period of 67 ms. An operating pulse width of 140 μ s was chosen so that the power supply operating voltage is under 10 kV and within the realm of semi-conductor switching devices and planar transmission lines. They will be pulsed from 10 to 15 times at the 15 Hz rate in one second followed by a rest period of one second. The sequence will be repeated on a continuous basis. This results in a system load current of 4730 A(rms) for 10 pulses and 5790 A(rms) for 15 pulses for the supply design peak current of 250 kA. The present operating plan is to run at a peak current of 170 kA and an average repetition rate of 5 pulses per second.

Circuit Requirements

A LC discharge circuit will be used as shown in Figure 3.27, which will achieve the peak current when the SCR switch releases stored energy from the capacitor bank into the horns via the stripline. The estimated circuit parameters are listed in Table 3.4. The power levels correspond to 170 kA, 5 Hz operation.

Current and voltage waveforms of a typical cycle of power supply operation are shown in Figure 3.28. The capacitor bank is initially charged to a positive voltage appropriate to 250 kA of output current. Upon command the stored energy will be switched into the focusing horns that make up the load. After the

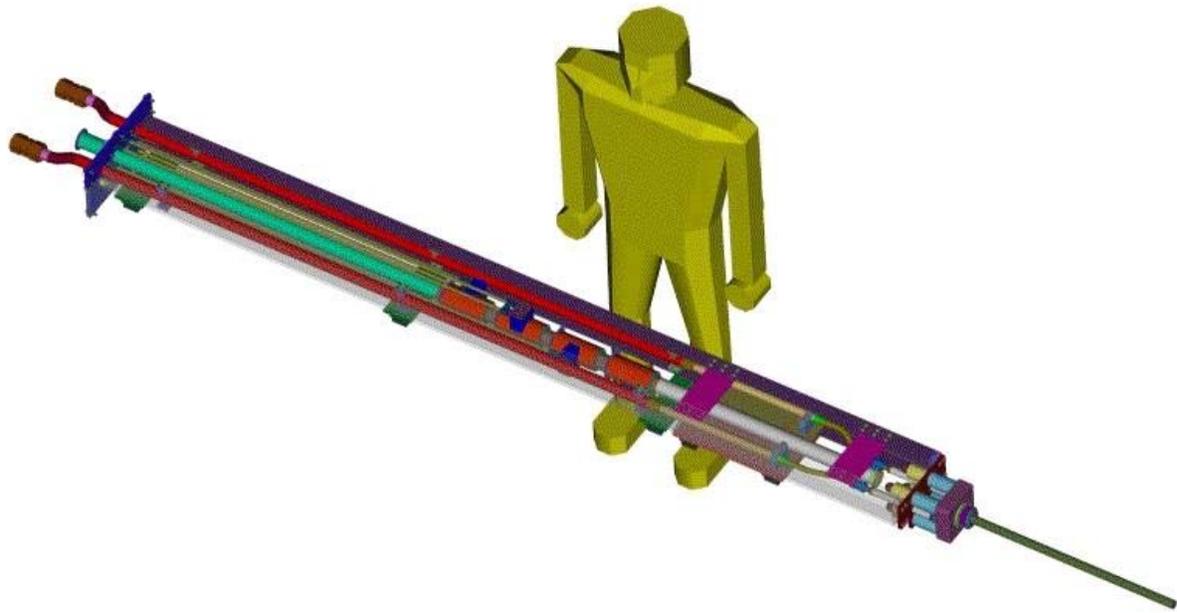


Figure 3.26: Overall view of the target module with man for scale. The right C-channel is rendered transparent to see the air tube routing inside the module.

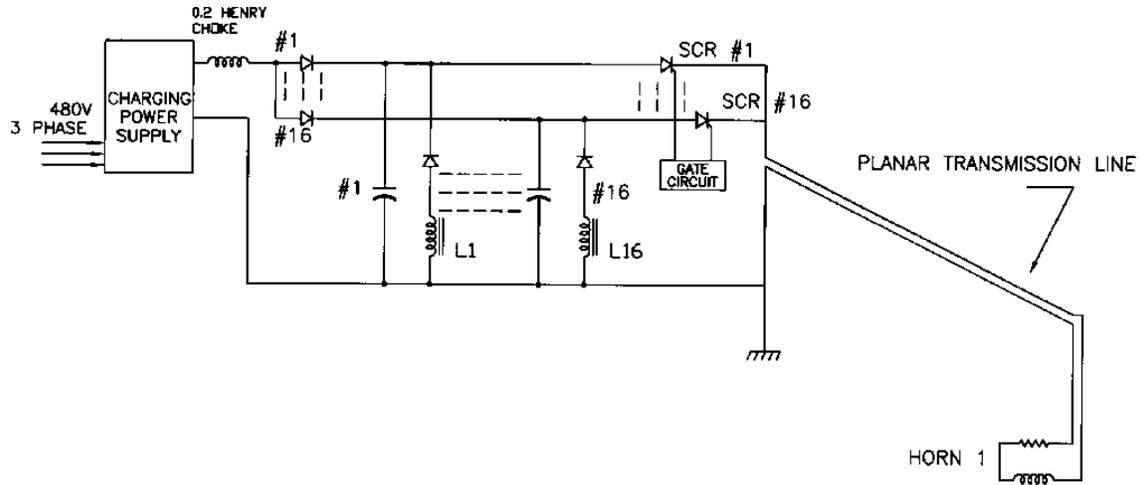


Figure 3.27: A LC discharge circuit that will achieve the peak current when the LCR switch releases stored energy from the capacitor bank into the horns via the stripline

Table 3.4: Horn circuit characteristics

Component	Inductance	Resistance	Power
Horn	0.70 μH	0.240 m Ω	2.5 kW
Stripline (20 meters)	0.26 μH	0.50 m Ω	5.0 kW
P.S. Cap. Bank plus losses	0.37 μH	3.0 m Ω	30 kW
Total	1.33 μH	3.74 m Ω	37.5 kW

discharge of energy into the horns, the capacitor bank will have reversed its polarity. To recover this energy, the capacitor bank is allowed to “ring” through a separate inductor via free-wheeling diodes, after which the capacitor bank polarity is in the forward direction. At the end of the recovery cycle the energy lost from the capacitor bank will be replaced by the charging power supply in time for the next discharge cycle to begin.

Capacitor Bank

From the inductance and resistance values projected for the two focusing horns and estimates for the balance of the circuit, the capacitance required for the bank is 1,350 μF at 10.5 kV. The total energy stored within the capacitor bank during operation is 61 kJ. This is made up of an array of individual energy storage capacitors connected in parallel but separated electrically into sixteen cells. The number of capacitors in each cell has been chosen to limit the amount of stored energy to a value that can be safely contained within an individual capacitor case, without rupture in the event of an internal fault.

Charging System

The capacitor bank will be recharged by a 168 kW switch-mode power supply array purchased from Maxwell Industries. The calculated average power consumption during operation of the horn is 37.5 kW. The required voltage for operation based upon present values for the circuit elements is 5.4 kV. Diodes are used between the charging power vsupply and the separate sections of the capacitor bank. This permits charging of each

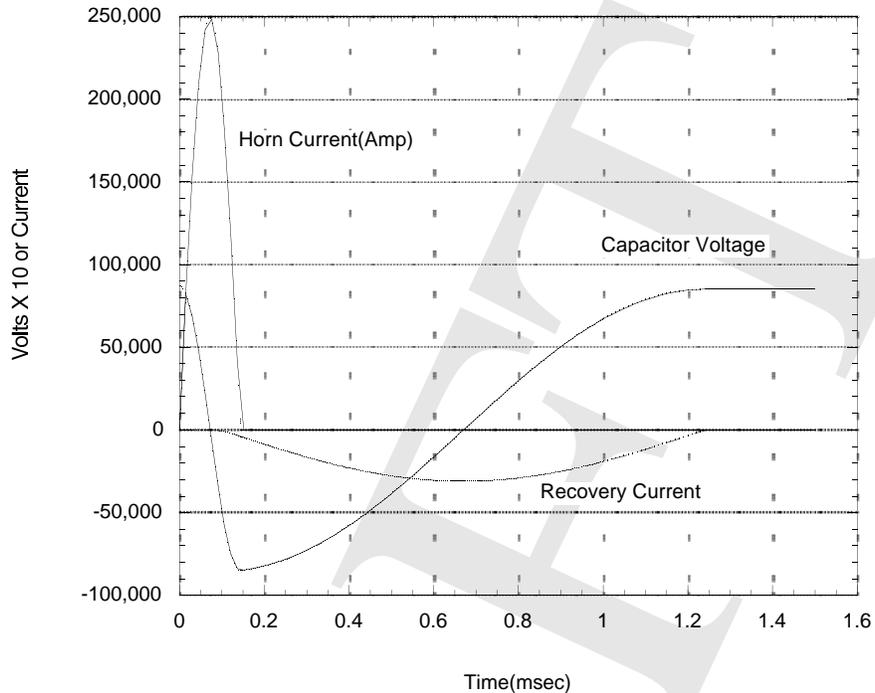


Figure 3.28: Current and voltage waveforms of a typical cycle of power supply operation

of the capacitor bank cells while keeping them isolated from one another for safety. The series diodes also prevent capacitor bank stored energy from being delivered backwards to the charging power supply in the event of a fault internal to the charging supply. These diodes are rated for the charging current level and twice the capacitor bank operating voltage.

Discharge resistors and safety system

A safety system will monitor operating parameters of the power supply and will shut it down if out-of-tolerance conditions are detected. Monitored parameters include overvoltage and overcurrent conditions of the charging supply, over voltage and over current conditions of the capacitor bank, ground fault currents, excessive temperatures, loss of cooling to the power supply or horn, personnel entry, etc. When fault conditions are detected, the charging supply will be turned off and the capacitor bank will be discharged via a redundant arrangement of dump resistors and shorting relays to remove the stored energy. The dump resistors will be rated to absorb the maximum stored energy capability of the capacitor bank, 74 kJ.

Discharge Switch

The discharge of stored energy from the capacitor bank to the horns is performed by SCRs. Each switching element consists of ten SCRs in a series assembly. Sixteen such assemblies working in parallel share in switching the total load current.

Current Transducers

Passive current transformers will be used to monitor the output current from the supply. This is done by using sixteen monitors, one associated with each switching element, with the outputs summed together to

read total current. This method has the advantage of allowing the monitoring of the performance of each capacitor bank cell/SCR combination.

Transmission line (WBS 2.1.14)

The transmission line (stripline) that brings power from the output of the power supply/capacitor bank to the horns consists of a ten-layer assembly of parallel plates. The overall cross section of the transmission line will be approximately 12" × 12", with individual plates being 3/8" × 12" of aluminum alloy type 6101. Plates are separated by ceramic insulators. The completed assembly is held in compression by clamps and bolts at the spacer locations.

Power losses in the line will be roughly equal to that of the two horns combined, 5 kW. The stripline is being constructed to carry 5790 A and capable of dissipating the resultant heat using a forced-air cooling system. In addition, it is insulated for 10 kV operation, allows for thermal expansion and contraction at the horn connections, has insulation tolerant to the high radiation fields that will be present near the horn, and permits rapid as well as reliable connection/disconnection at the horn.

Cabinets

Cabinets similar to that used for the recently completed TESLA Modulators have been procured for this power supply. They total 7' high × 27' long × 7' deep.

Chapter 4

The Neutrino Flux

The neutrino flux which results from the above technical design meets the MiniBooNE experimental goals. In this chapter we describe the neutrino flux which results from the technical design described in the previous two chapters. Here we assume two calendar years of Booster running (10^{21} pot), equally divided between absorber positions of 50 m and at 25 m. In order to obtain these fluxes, the spot size and divergence for a 20π Booster emittance was used as input to a GEANT-based full simulation of the target, horn and decay region. The simulation is based upon the GEANT [20] transport code with the standard FLUKA hadron interaction package activated. All beamline elements, including the horns, shielding, and absorbers, were simulated.

4.1 The ν_μ Flux

For a low energy neutrino beam, there is a trade-off between statistics and low average beam energy. High energy neutrinos have a larger interaction cross-section and thus provide more neutrino events, but the larger neutral current π^0 cross-section and the larger ν_e flux at these energies also enhance background. This, along with the increased reliability of the components, was a key consideration in selecting the one-horn, lower-current design described in Chap. 3.

The ν_μ flux at 500m for a detector on the z -axis with 6m radius is shown as the solid histogram in Fig. 4.1. Using a gaussian fit, the peak of the spectrum is at 0.94 GeV. Forty-eight percent of the spectrum is in the optimal range, between 0.3 and 1.0 GeV.

The case of perfect focusing, where all pions produced in the target go down the central z axis, is often used as a benchmark. It is indicated by the solid histogram on Fig. 4.2. The integrated flux is roughly one-fourth of perfect focusing. This is typically what can be achieved from an optimized single-horn system; the NuMI two-horn design in its high-energy configuration is expected to achieve a higher fraction [25].

A study of the variation in the neutrino flux with beam parameters has been carried out and the design was found to be robust. Variation in horn current by 50kA results in a change of flux of 12%. Beam displacement of 2mm results in a loss of flux of 13% [1].

In the present design, the decay pipe is filled with air. The improvement in flux if the pipe were evacuated or filled with helium is only 3.0-3.5%, which was deemed too small to warrant the cost and maintenance complications of a vacuum or helium system.

4.2 The ν_e Background

A ν_e background is inevitable in this experiment. What is important is that the ν_e background be as small as possible and be well understood. In addition, one wants the energy dependence of the ν_e background to be significantly different from that of the signal.

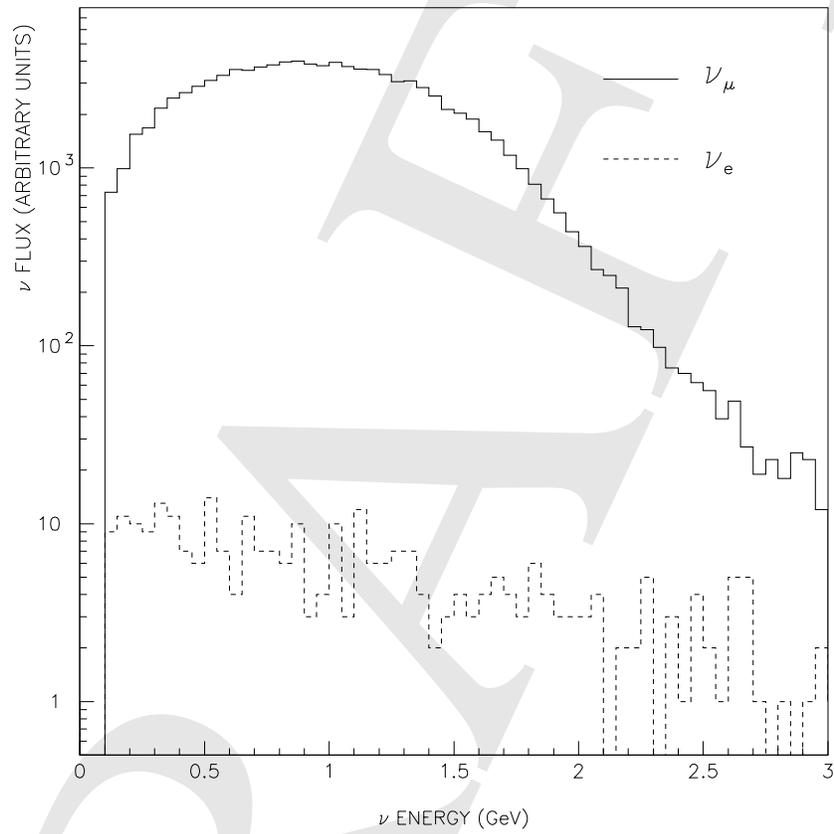


Figure 4.1: The ν_μ flux (solid) at the MiniBooNE detector compared to the ν_e background (dashed).

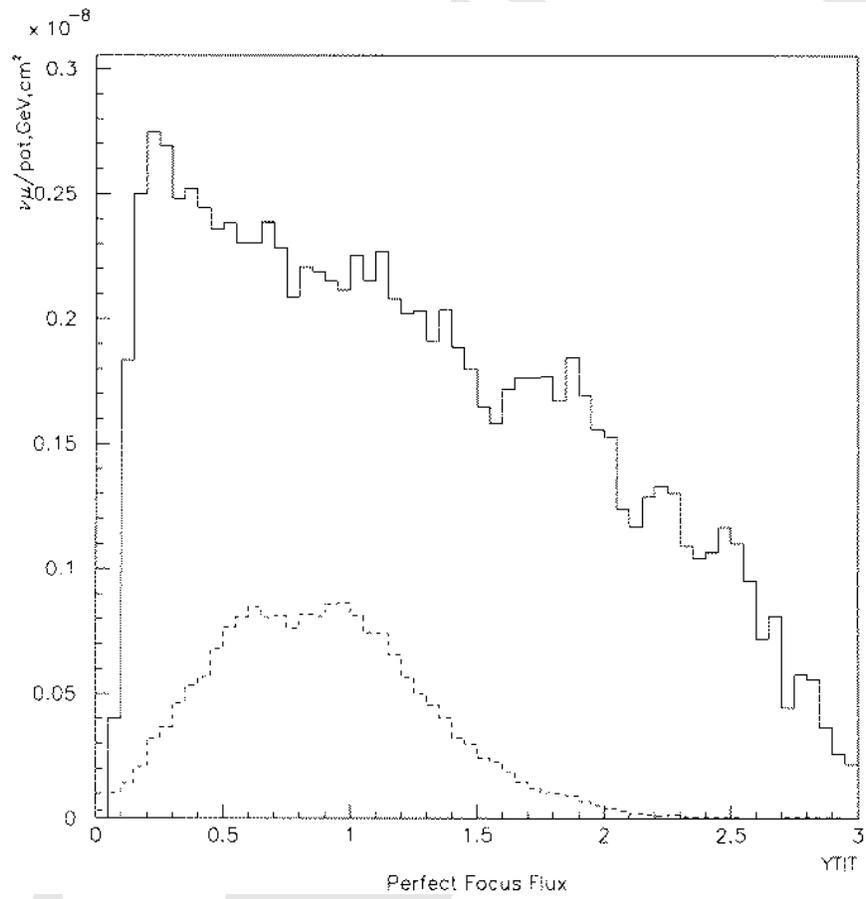


Figure 4.2: The ν_{μ} flux for the MiniBooNE horn system (dashed) compared to perfect focusing (solid).

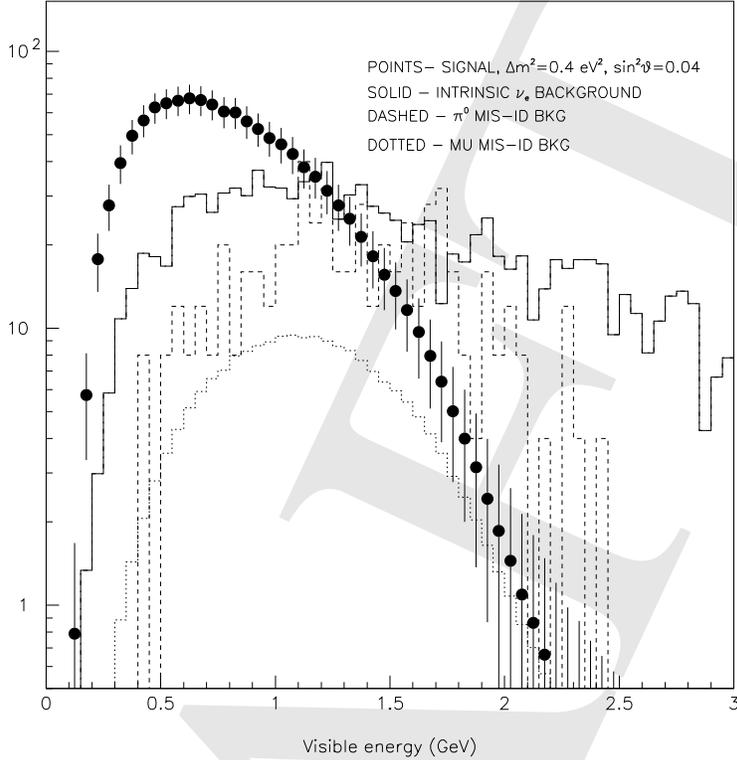


Figure 4.3: The energy dependence of the ν_e beam background compared to a hypothetical oscillation signal. The parameters for the signal are $\Delta m^2=0.4 \text{ eV}^2$ and $\sin^2 2\theta = 0.04$. The statistical fluctuations in the background histograms reflect limited Monte Carlo statistics; the error bars on the signal points indicate the size of the expected statistical error with 10^{21} protons on target.

The expected ν_e background is shown by the dashed histogram on Figure 4.1. This background is 0.2% of the ν_μ flux. Of these background events, approximately half are due to muon decays and half from K decays. (About 80% of the kaon-induced ν_e come from K_{e3}^+ decays, the remainder from K_{e3}^0 .) While kaons have a shorter decay length than muons, the kaons' production rate is low for 8 GeV primary protons, resulting in roughly equal backgrounds from each source. The ν_e from muon decays can be determined through several methods[1], and therefore the systematic uncertainty on this background is estimated to be 5%. Our understanding of the background from kaons will rely on Monte Carlo estimates which are tied to high precision low energy production experiments [1] and to data from the Little Muon Counters (LMC, Sec.3.2.2). The systematic error on K -decay ν_e is estimated to be 10%.

An important feature of the MiniBooNE neutrino beam is that the ν_e background has a different energy dependence from that expected for oscillations. For example, Figure 4.3 compares the ν_e background to a hypothetical $\nu_\mu \rightarrow \nu_e$ oscillation signal, with $\Delta m^2=0.4 \text{ eV}^2$ and $\sin^2 2\theta = 0.04$. The signal is indicated by the data points, with expected systematic and statistical errors on the measurement indicated by the bars. The ν_e background is indicated by a curve, with the systematic error on the ν_e background shown by the band. The energy dependences are substantially different.

4.3 Comparison to the Design Goal

The beam presented in this TDR, fully modeled by GEANT, including all shielding, meets our design goals as presented in the proposal. We have calculated the sensitivity using the same detector considerations as in the proposal, but with the realistic beam presented in this document and detection efficiencies based on a realistic detector Monte Carlo simulation. The resulting sensitivity is presented in Fig. 4.4 as the solid curve. This is compared to the proposal sensitivity, shown in Fig. 4.4 as the dashed curve. Note that these sensitivities are calculated without detailed consideration of energy dependence of the background. Therefore, they represent a conservative estimate of the sensitivity. Expected statistical errors and systematic errors on the background components are included.

The goal was to obtain over an order of magnitude more events than LSND's "golden" sample. From 1993 through 1998, LSND obtained 39.5 ± 8.8 excess events (*preliminary*). In order to compare MiniBooNE expectations, we consider two $(\sin^2 2\theta, \Delta m^2)$ points which represent extremes of the allowed LSND region. For $\sin^2 2\theta = 0.03$ and $\Delta m^2 = 0.3\text{eV}^2$, MiniBooNE will obtain 523 events before an energy cut (382 after a cut on reconstructed ν_e energy $E_{vis} < 1$ GeV), an 11.8σ signal. For $\sin^2 2\theta = 0.002$ and $\Delta m^2 = 2.0\text{eV}^2$, MiniBooNE will obtain 484 events before the energy cut (220 after), a 6.8σ signal. These event rates are well over an order of magnitude greater than the 39 LSND excess "golden events." These event rates are 40 ~ 70% of the proposal event rates, although reduced background levels allow the physics sensitivity to remain similar. The loss in events is due to increases in shielding in the target pile and decay region, the decision to use a single focusing horn rather than a two-horn system, and reconstruction optimization to reduce the backgrounds. Indeed, after the 1 GeV energy cut, the total background is only 681 events and is far less dominated by the hard-to-understand ν_e from kaon decay.

The aim of the optimized horn and decay region design was to reduce the ν_e background in the beam from the 0.3% level of the proposal. This is important to prevent systematic errors from dominating the statistical errors in the oscillation analysis. The ν_e background for the beam presented in this TDR is 0.26% (0.021% after the $E_{vis} < 1$ GeV cut). The ν_e 's from muon and K_L^0 decay have been reduced by tuning the pion spectrum of the horns and by reducing the aperture of the decay region; the ν_e 's from K^+ and K_L^0 decay have been further reduced by the energy cut in the analysis.

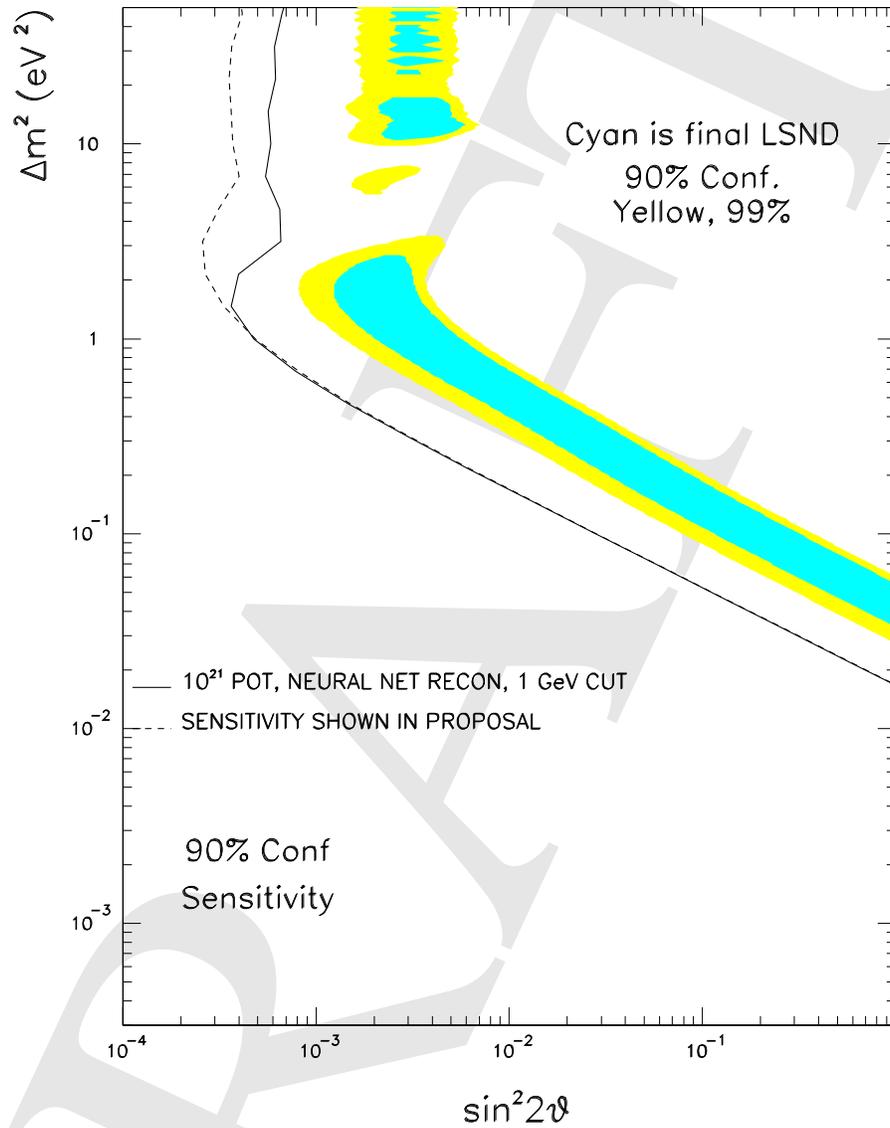


Figure 4.4: The sensitivity of the MiniBooNE designed beam compared to the final results from LSND. The solid curve represents the expected 90% confidence level limit from E898 if there is no signal. The analysis removes events with an equivalent electron energy greater than 1 GeV. The sensitivity from the original E898 proposal is shown as the dashed curve.